



UNIVERSITAT POLITÈCNICA DE CATALUNYA
BARCELONATECH
Escola d'Enginyeria de Barcelona Est

FINAL MASTER'S THESIS

**Master's degree in Chemical Engineering - Smart Chemical
Factories**

**A SIMULATION APPROACH TO THE IMPROVEMENT OF THE
DOSAGE OF HYDROGEN PEROXIDE FOR PHOTO-FENTON
PROCESSES**



Report

Author: Marta Costa de Aguirre
Director: Moisès Graells Sobré
Co-Director: Montserrat Pérez-Moya
Call: June 2022

Resum

L'objectiu d'aquest treball és contribuir a un tractament d'aigües més eficient i sostenible. El procés foto-Fenton ha demostrat ser molt eficient per al tractament d'aigües recalcitrants i no biodegradables. Diverses investigacions han demostrat la importància de la dosificació de peròxid d'hidrogen (H_2O_2) en la millora del rendiment del procés, ja que pot evitar o reduir l'activació de reaccions ineficients. Per trobar la dosificació òptima, no és possible provar experimentalment tots els tipus de dosificació, per la qual cosa cal desenvolupar i implementar un model que pugui predir el procés.

En aquest projecte s'ha explotat un model dinàmic de foto-Fenton que inclou el subministrament flexible de peròxid d'hidrogen per determinar un perfil de dosificació millorat per a un tractament foto-Fenton determinat. S'adopta del treball presentat per Nasr Esfahani et al., (2022), en què es va ampliar i adoptar el model foto-Fenton de Cabrera-Reina et al. (2012) i Audino et al. (2019). Utilitza les dades experimentals obtingudes per Yu et al., (2020) utilitzant diferents esquemes de dosificació per a la mineralització de solucions de paracetamol (PCT) a escala de planta pilot.

Després de validar el model amb alguns dels experiments utilitzats per al calibratge, es va realitzar la seva explotació simulant noves situacions ampliant els rangs de les variables de decisió en comparació dels experiments de Yu et al., (2020). El temps de reacció, la quantitat total de peròxid d'hidrogen i el perfil de dosificació van ser les variables utilitzades per a la presa de decisions. L'anàlisi i la discussió dels resultats es van fer principalment utilitzant les concentracions de peròxid d'hidrogen, el carboni orgànic total (COT) i l'oxigen dissolt (OD). Les concentracions d'OD permeten una explicació més completa de la naturalesa del procés.

Dins de les situacions estudiades, els resultats de les simulacions van mostrar que el perfil de dosificació tenia poc efecte a la mineralització final. En augmentar el temps del procés, es van observar millores significatives en la mineralització dels contaminants, així com quan es va augmentar la quantitat de peròxid d'hidrogen, encara que l'experiència i la literatura desaconsellen afegir massa oxidant per tenir un bon rendiment.

De la simulació es van seleccionar dues de les estratègies millorades per ser validades a la planta pilot. L'objectiu del primer experiment era comprovar l'efecte positiu en l'eliminació de COT de l'addició d'una quantitat de peròxid d'hidrogen superior a l'estequiomètrica. Com era d'esperar i d'acord amb l'experiència i la literatura, afegir massa oxidant no va millorar els resultats de mineralització a la planta pilot.

El segon experiment volia comprovar si l'augment del temps de reacció mentre s'utilitzava la quantitat estequiomètrica total de H_2O_2 beneficiaria els resultats. En aquest cas, els resultats de les simulacions

sí que van coincidir amb els de la planta pilot, obtenint una mineralització del 80%. Així doncs, utilitzant el model s'ha trobat una estratègia de dosificació més eficaç.

Resumen

El objetivo de este trabajo es contribuir a un tratamiento de aguas más eficiente y sostenible. El proceso foto-Fenton ha demostrado ser altamente eficiente para el tratamiento de aguas recalcitrantes y no biodegradables. Varias investigaciones han demostrado la importancia de la dosis de peróxido de hidrógeno (H_2O_2) en la mejora del rendimiento del proceso, ya que puede evitar o reducir la activación de reacciones ineficientes. Para encontrar la dosis óptima, no es posible probar experimentalmente todos los tipos de dosis, por lo que es necesario desarrollar e implementar un modelo que pueda predecir el proceso.

En este proyecto se ha explotado un modelo dinámico de foto-Fenton que incluye el suministro flexible de peróxido de hidrógeno para determinar un perfil de dosificación mejorado para un tratamiento foto-Fenton determinado. Se adopta del trabajo presentado por Nasr Esfahani et al., (2022), en el que se amplió y adoptó el modelo foto-Fenton de Cabrera-Reina et al. (2012) y Audino et al. (2019). Utiliza los datos experimentales obtenidos por Yu et al., (2020) utilizando diferentes esquemas de dosificación para la mineralización de soluciones de paracetamol (PCT) a escala de planta piloto.

Después de validar el modelo con algunos de los experimentos utilizados para su calibración, se realizó su explotación simulando nuevas situaciones ampliando los rangos de las variables de decisión con respecto a las de los experimentos de Yu et al., (2020). El tiempo de reacción, la cantidad total de peróxido de hidrógeno y el perfil de dosificación fueron las variables utilizadas para la toma de decisiones. El análisis y la discusión de los resultados se realizaron principalmente utilizando las concentraciones de peróxido de hidrógeno, el carbono orgánico total (COT) y el oxígeno disuelto (OD). Las concentraciones de OD permiten una explicación más completa de la naturaleza del proceso.

Dentro de las situaciones estudiadas, los resultados de las simulaciones mostraron que el perfil de dosificación tenía poco efecto en la mineralización final. Al aumentar el tiempo del proceso, se observaron mejoras significativas en la mineralización de los contaminantes, así como cuando se aumentó la cantidad de peróxido de hidrógeno, aunque la experiencia y la literatura desaconsejan añadir demasiado oxidante para tener un buen rendimiento.

De la simulación se seleccionaron dos de las estrategias mejoradas para ser validadas en la planta piloto. El objetivo del primer experimento era comprobar el efecto positivo en la eliminación de COT de la adición de una cantidad de peróxido de hidrógeno superior a la estequiométrica. Como era de esperar y de acuerdo con la experiencia y la literatura, añadir demasiado oxidante no mejoró los resultados de mineralización en la planta piloto.

El segundo experimento quería comprobar si el aumento del tiempo de reacción mientras se utilizaba la cantidad estequiométrica total de H_2O_2 beneficiaría los resultados. En este caso, los resultados de

las simulaciones sí coincidieron con los de la planta piloto, obteniendo una mineralización del 80%. Por consiguiente, utilizando el modelo, se ha encontrado una estrategia de dosificación más eficaz.

Abstract

The aim of this work is to contribute to more efficient and sustainable water treatment. The photo-Fenton process has proven to be highly efficient for treating recalcitrant and non-biodegradable waters. Several researches have shown the significance of hydrogen peroxide (H_2O_2) dosage in the improvement of the process performance, since it can avoid or reduce the activation of inefficient reactions. In order to find the optimal dosage, it is not possible to experimentally test all types of dosages, thus it is necessary to develop and implement a model that can predict the process.

This project has exploited a dynamic photo-Fenton model including flexible hydrogen peroxide supply to determine an improved dosage profile for a given photo-Fenton treatment. It is adopted from the work presented by Nasr Esfahani et al., (2022), in which the photo-Fenton model by Cabrera-Reina et al. (2012) and Audino et al. (2019) was extended and adopted. It uses the experimental data obtained by Yu et al., (2020) using different dosage schemes for the mineralization of paracetamol (PCT) solutions at a pilot plant scale.

After validating the model with certain of the experiments used for its calibration, its exploitation was performed by simulating new situations by extending the ranges of the decision variables from those of the Yu et al., (2020) experiments. Reaction time, total amount of hydrogen peroxide and dosing profile were the variables used for decision making. Analysis and discussion of the results were conducted mainly using hydrogen peroxide concentrations, Total Organic Carbon (TOC) and dissolved oxygen (DO). DO concentrations allow for a more comprehensive explanation of the nature of the process.

Within the studied situations, the results of the simulations showed that the dosing profile had little effect on the final mineralization. By increasing the process time, significant improvements in pollutant mineralization were observed, as well as when the amount of hydrogen peroxide was increase, even experience and literature advise against adding too much oxidant to have a good performance.

Two of the improved strategies were selected from the simulation to be validated in the pilot plant. The aim of the first experiment was to check the positive effect on TOC removal of adding more than the stoichiometric amount of hydrogen peroxide. As expected and according to experience and literature, adding too much oxidant did not improve mineralization results in the pilot plant.

The second experiment aimed to check whether increase of the reaction time while using the total stoichiometric amount of H_2O_2 would benefit the results. In this case, the results of the simulations did match those of the pilot plant, obtaining a mineralization of 80%. Hence, by using the model, a more effective dosing strategy was found.



Acknowledgments

First and foremost, I would like to express my deepest gratitude to my project supervisors, Moisès Graells and Montserrat Pérez-Moya, for their guidance and support throughout the entire project at the research group CEPIMA (Centre d'Enginyeria de Processos i Medi Ambient).

I would like to extend my gratitude to all the members from CEPIMA, for their commitment and welcoming attitude towards me when I first join the group. In particular, I would like to express my appreciation to PhD student Kourosh Nasr Esfahani, for the help and interest for the project and to give me advice and knowledge with respect some of the topics developed on the project.

Furthermore, I would like to extend my deepest thanks to my family and friends because this project would not have been possible without their endless patience, love and helpfulness. Their support during the entire studies has given me strength in the most challenging moments.



Glossary

CHEMICAL NOTATION

$C_8H_9NO_2$	Paracetamol
Fe^{2+}	Ferrous ion
Fe^{3+}	Ferric ion
$FeSO_4 \cdot 7H_2O$	Iron sulphate
H^+	Hydron
H_2O_2	Hydrogen peroxide
H_2SO_4	Sulphuric acid
H_3PO_4	Phosphoric acid
O_2	Oxygen
OH^-	Hydroxide
OH^\cdot	Hydroxyl radical
VO_2^{3+}	Peroxovanadium cation
VO_3^-	Ammonium metavanadate

GENERAL NOMENCLATURE

$A(t)$	Amount of H_2O_2 employed at a given time t	mmol, mL
$A(\tau)$	Total amount of H_2O_2 added	mmol, mL
$[C_i]$	Concentration of the component inside the reactor	mmol L^{-1} , mg L^{-1}
$[C_i]^*$	Saturation concentration	mmol L^{-1} , mg L^{-1}
$[C_i]_0$	Initial concentration of the component	mmol L^{-1} , mg L^{-1}

$[C_i]_{in}$	Concentration of the component in the inlet flow rate	mmol L ⁻¹ , mg L ⁻¹
c_1	Stoichiometric coefficient in the dissolved oxygen balance	
EXP1	First experiment performed in the pilot plant	
EXP2	Second experiment performed in the pilot plant	
$F(t)$	Inlet flowrate	mmol min ⁻¹
g_1	Stoichiometric coefficient in the dissolved oxygen balance	
g_2	Stoichiometric coefficient in the dissolved oxygen balance	
i	General component	
k_1 to k_9	Kinetic constants for each reaction	several units
K_{1a}	Gas-liquid mass transfer coefficient in the dissolved oxygen	h ⁻¹
M	Parent organic compound present at the beginning of the reaction	
MX_1	Partially oxidized organic: first intermediate	
MX_2	Partially oxidized organic: second intermediate	
n	Section in piecewise function	
R	Free radicals	
S	Stoichiometric H ₂ O ₂ amount to oxidize 0.2646 mmol C ₈ H ₉ NO ₂	mmol, mL
T	Temperature	°C
V	Total volume of the reactor	L

GREEK SYMBOLS

τ	Final reaction time (reaction span)	h, min
--------	-------------------------------------	--------

$\chi(\%)$	TOC conversion in %
$\chi(\tau)$	TOC conversion at the final time τ

ACRONYMS

ACR	Model by Cabrera-Reina et al., (2012)
ANN	Artificial Neural Network
AOP	Advanced Oxidation Processes
BOD	Biochemical Oxygen Demand
CEC	Contaminants of Emerging Concern
CEPIMA	Center for Process and Environmental Engineering
COD	Chemical Oxygen Demand
DBM	Data Based Model
EM	Empirical Model
FAU	Model by Audino et al., (2019)
FPM	First Principle Modelling
KNE	Model by Nasr Esfahani et al., (2022)
MATLAB	MATrix LABoratory
NDIR	Non Dispersive Infrared
ODEs	Ordinary Differential Equations
ORP	Oxidation Reduction Potential
PCT	Paracetamol
PID	Proportional-Integral-Derivative

PLC	Programmable Logic Controller
RWWS	Recalcitrant Wastewaters
SCADA	Supervisory and Control And Data Acquisition System
SDG	Sustainable Development Goal
SEM	Semi Empirical Models
TC	Total Carbon
TIC	Total Inorganic Carbon
TOC	Total Organic Carbon
UN	United Nations
UV	Ultraviolet
WWTP	Wastewater Treatment Plant
XYU	Yu et al.,(2020) work



Index

Resum.....	II
Resumen	IV
Abstract.....	VI
Acknowledgments	VIII
Glossary.....	X
1 PREFACE	1
1.1. Project's background	1
1.2. Motivation and scope of the project.....	1
2 INTRODUCTION	2
3 OBJECTIVES AND SCOPE	4
3.1 Stages of the project.....	4
4 STATE OF THE ART	6
4.1 Advanced Oxidation Processes (AOPs).....	6
4.1.1 Fenton and Photo-Fenton processes	7
4.2 Mathematical modelling of chemical processes	10
4.2.1 Literature review of photo-Fenton processes modelling	11
5 PHOTO-FENTON MODEL	13
5.1 Kinetic and reactor model	13
5.2 Reference data.....	17
5.3 Global sensitivity analysis (GSA) and parameter estimation	18
5.4 Mathematical tools.....	19
5.4.1 Simulation methodology	20
6 EXPERIMENTAL METHODS	23
6.1 Experimental setting.....	23
6.1.1 Fenton/Photo Fenton pilot-plant.....	23
6.1.2 Reagents and chemicals	26
6.2 Analytical techniques.....	27
6.2.1 Total Organic Carbon (TOC) determination	27
6.2.2 Hydrogen peroxide determination via spectrophotometric technique.....	28
6.3 Pilot-plant experiments	29

7	RESULTS AND DISCUSSION	31
7.1	Preliminary simulation results	31
7.2	Model exploitation results and discussion	39
7.3	Experimental results and discussion	48
8	CONCLUSIONS	52
9	REFERENCES	55

1 Preface

1.1. Project's background

The project continues the work presented by Nasr Esfahani et al., (2022), in which the photo-Fenton model by Cabrera-Reina et al. (2012) and Audino et al. (2019) was extended and adopted. This project contributes a practical model aimed at providing model-based optimization for the H₂O₂ dosage profile of the photo-Fenton process, and uses the experimental data obtained by Yu et al., (2020) using different dosage schemes for the mineralization of paracetamol (PCT) solutions at a pilot plant scale. Hence, the same case study presented by Nasr Esfahani et al., (2022) will be developed and exploited.

1.2. Motivation and scope of the project

Experimental approaches are essential to providing the necessary insight to the mechanisms involved in the efficient use of hydrogen peroxide, but the exploration and assessment of all possible dosage profiles cannot be attempted experimentally.

In this regard, researchers have studied the photo-Fenton process with the dosage of hydrogen peroxide to enhance process performance. The sequential addition of H₂O₂ along the reaction span has been shown to improve mineralization (Santos-Juanes et al., 2011). However, determining an appropriate dosage cannot be limited to a pre-determined recipe; it should ideally include some process feed-back in order to robustly adapt to process disturbances and/or model mismatch. It is important to emphasize that the H₂O₂ dosage strategy is essential for competitiveness of the photo-Fenton process because H₂O₂ is the most expensive reagent (Yu et al., 2021). Therefore, the key research issue is to optimize a model-based, time-dependent H₂O₂ dose profile to maximize process performance while reducing scavenging effects by employing acceptable hydrogen peroxide supply.

The purpose of the project was to contribute to the development of a systematic modelling approach that would allow for more efficient and sustainable-term water management. Hence, this project has exploited a dynamic photo-Fenton model including flexible hydrogen peroxide supply to determine an improved dosage profile for a given photo-Fenton treatment.

2 Introduction

Water and sanitation are at the core of sustainable development, and the range of services they provide underpin poverty reduction, economic growth and environmental sustainability. However, in recent decades overexploitation, pollution, and climate change have led to severe water stress in locales across the world. According to the United Nations (UN) sixth Sustainable Development Goal (SDG) “Ensure availability and sustainable management of water and sanitation for all”, urgent action is needed to overcome this global crisis, as it is affecting all countries around the world, socially, economically and environmentally (*Water and Sanitation | Department of Economic and Social Affairs, 2022*).

On one hand, due to the high demand of aquaculture commodities and insufficiency of capture fishery, approaches for intensification of the aquaculture sector have become major topics of interest (Babatunde Dauda et al., 2019). The transformation of aqua farming process involves innovations in chemicals used for boosting production. Fertilizers, water conditioners, hormones, antifungal compounds, and antibiotics are among these chemicals. These chemicals were not used in old conventional culture systems and innovations are under continuous development (FAO, 2018).

Further to this, the actual population has developed, mainly in modern cities, different ways to reach a certain level of comfort for the daily life. To satisfy this level of convenience, food (crops, cattle, processed food) and industrial (hydrocarbons, pharmaceuticals, electronics) production has increased, as well as the development of new synthetic products (xenobiotics) (Sanchez-Salas et al., 2018).

Because of these and other human activities, chemical compounds are released into wastewaters as a result of the use of newly introduced chemicals. These compounds are rarely known in contrast to other parameters, such as organic and turbid materials, suspended solids, nitrogen, and phosphorus, which are well-known constituents in aquaculture wastewater (Ahmad et al., 2022). In addition, some of these new compounds are considered recalcitrant or non-biodegradable. Due to their detrimental impacts, persistence, and biomagnification in natural and human habitats, recalcitrant pollutants such as hydrocarbons, pesticides, certain personal care items, nanomaterials, and many forms of toxins are on the rise and gaining increased attention.

Among these substances there are the Contaminants of Emerging Concern (CECs), a group of unregulated chemicals that may be candidates for future legislation, depending on the outcomes of research into their impacts on human health, aquatic life forms, and environmental presence. The European Parliament and the Council adopted Directive 2013/39/EU on the 12th of August 2013, amending Directives 2000/60/EC and 2008/105/EC, which addresses the issue of priority substances in water policy, emphasizes the importance of CECs monitoring, and updates the list of priority

substances (Ribeiro et al., 2015). Detergents, pharmaceutical products and its metabolites, antiseptics, fragrances, industrial additives, personal care products, flame retardants, steroids and hormones, are classified as particularly relevant emerging contaminants (Figure 1).

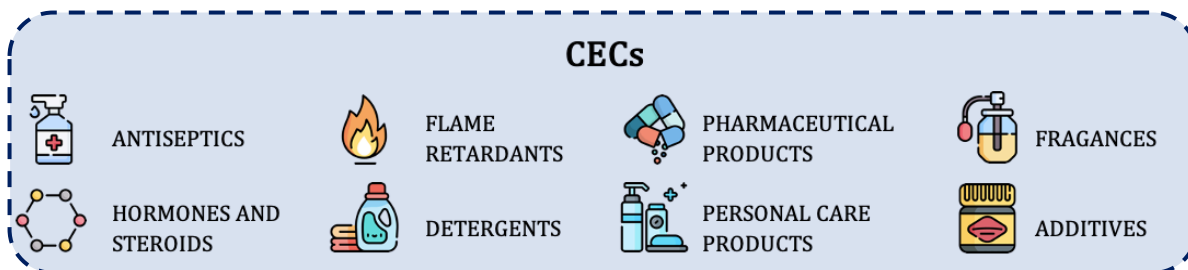


Figure 1: Most relevant Contaminants of Emerging Concern.

CECs are increasingly being detected at low concentrations (ng L^{-1} to $\mu\text{g L}^{-1}$) in surface waters, ground waters and even drinking waters. The main characteristic of this group of pollutants is that they are hardly biodegradable and consequently resist treatment by conventional wastewater treatment plants (WWTP). Thus, they are continuously and increasingly discharged into the environment (Sanchez-Salas et al., 2018).

Advanced oxidation processes (AOPs) have evolved as an efficient alternative for dealing with the degradation of these compounds, prompting considerable attention in the development and implementation of these technologies as final on-site treatments (for industrial wastewater) or as coupling treatment in activated sludge plant operations (for urban wastewater) (Elmolla & Chaudhuri, 2011).

Although AOPs are considered clean technology for this problem, they are also costly due to energy and chemical reagent usage, which increases with treatment time. As a result, achieving a practical implementation of AOPs is necessary.

According to a recent review (Oller, Malato, & Sánchez-pérez, 2011), the AOP area requires the development of more accurate economic models for cost estimates of coupled systems, as well as advancements in degradation kinetics and reactor modelling. Furthermore, the literature research revealed that while much effort was put into investigating AOPs using an experimental method, less work was put into finding the best design, operational and control, as well as automation of AOPs (Ortega-gómez et al., 2012; Yamal-Turbay et al., 2015).

3 Objectives and scope

The aim of this project is to contribute to improving the hydrogen peroxide dosing strategies in the photo-Fenton process in order to obtain higher efficiency results. Accordingly, the objectives of the present project are defined as follows:

- Analyze the model by Nasr Esfahani et al., (2022), from now on KNE, to verify to which extent it can adequately predict the evolution of the experiments with which it was calibrated
- Exploit the KNE model by simulating new situations by extending the ranges of the decision variables:
 - Identify the decision variables
 - Examine the effect of new operational decisions on the process performance
- Propose improved dosing strategies according to the following partial objectives:
 - Maximization of the final pollutant mineralization
 - Minimization of the process time
 - Minimization of the total amount of hydrogen peroxide required
- Validate at pilot-plant scale certain of the improved dosing strategies according to simulation

3.1 Stages of the project

As highlighted in Figure 2, the proposed stages of the project consist of different steps: validating a proposed model, exploiting it, finding dosages showing improvements and validating certain of these high-performing scenarios in a pilot plant. All of them will be discussed in detail in the following sections.

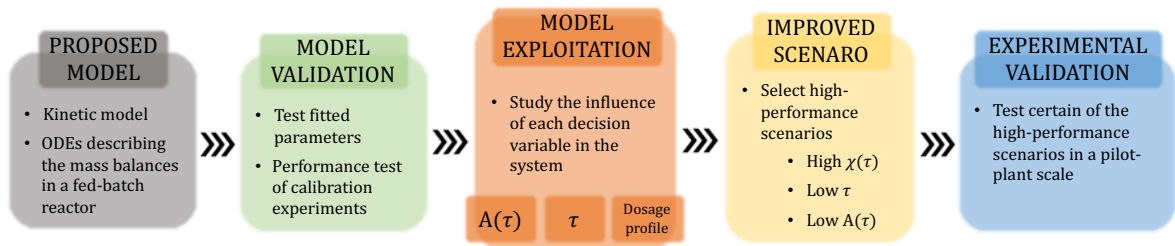


Figure 2: Stages of the project.

4 State of the art

This chapter presents a literature review of the different available water treatments. The review mainly focuses on Advanced Oxidation Processes (AOPs) and more specifically on Fenton and photo-Fenton processes.

Apart from that, different approaches from literature for the mathematical modelling of the photo-Fenton are further detailed.

4.1 Advanced Oxidation Processes (AOPs)

AOPs are a collection of chemical processes that can use the high reactivity of free radicals (e.g., HO• radicals) to drive oxidation reactions that can help with pollution removal and organic matter mineralization (Andreozzi et al., 1999). The HO• radicals are very reactive, attacking the majority of organic compounds at rates ranging from 10^6 to 10^9 L mol⁻¹ s⁻¹ (Farhataziz, A; Ross, 1977).

As a result, AOPs have been used at various scales for a variety of applications, including the sludge treatment (da Rocha et al., 2010; Pham et al., 2010), destruction of micropollutants (Ortega-Gómez et al., 2013; Prieto-Rodríguez et al., 2013) and specific pollutants (Babuponnusami & Muthukumar, 2012; Nichela et al., 2013; M. Tokumura et al., 2009), increase of biodegradability of recalcitrant wastewaters (RWWS) (Vilar et al., 2012), mineralization of organic matter (Ji et al., 2011) , and color and odor removal (Masahiro Tokumura et al., 2013).

HO• radicals also possess a low attack selectivity, allowing the use of such processes to effectively treat different contaminants. As a consequence, AOPs are currently considered to be the only feasible option for the treatment of refractory or toxic substances that can resist or damage conventional secondary biological treatments (Oller, Malato, & Sánchez-Pérez, 2011).

Nevertheless, chemical oxidation for complete mineralization of organic matter is an expensive solution because the intermediates by-products become more resistant during the oxidation process, necessitating a longer reaction time, increasing reagent and energy consumption, and thus increasing operational costs (Audino, 2019). Traditional biological processes, on the other hand, are more controllable and less expensive technologies.

As a result, the combination of traditional biological processes with AOPs has been presented as a potentially viable solution for lowering operational expenses. Pre-treatments using AOPs can be utilized to transform persistent or toxic pollutants into more biodegradable compounds. In this case, the goal is to determine the shortest possible pre-treatment time to achieve the desired level of

mineralization, ensuring the generation of biodegradable substances that can be treated with the subsequent biological treatment step while avoiding unnecessary chemical and energy consumption.

Furthermore, AOPs can be employed as a post-treatment step after secondary treatment in order to achieve a higher treatment quality level.

In the following scheme are the primary distinct options given by AOPs (Figure 3):

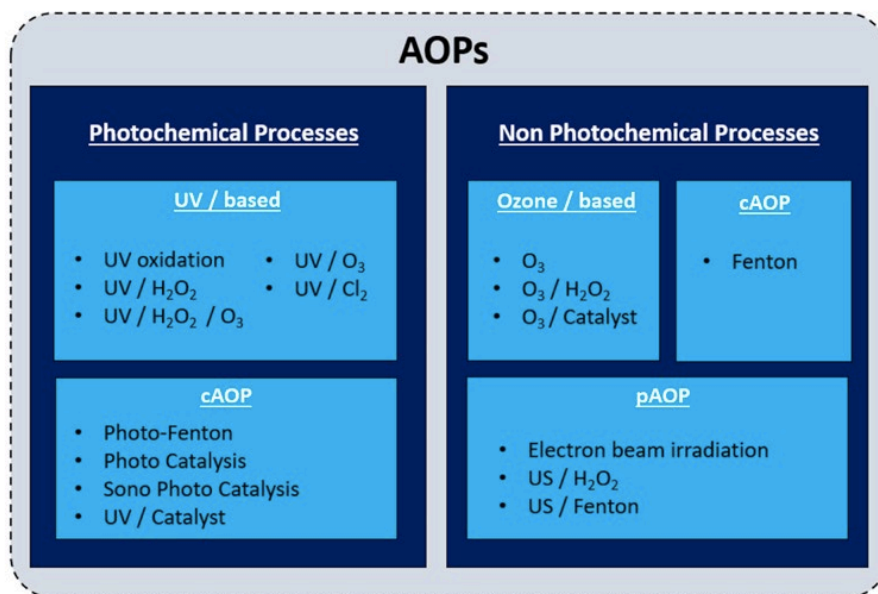


Figure 3: Classification of some common AOPs (cAOP = Catalytical AOP, pAOP = physical AOP) (Taoufik et al., 2021).

Among the existing AOPs, Fenton-like processes have proven to be highly efficient in the treatment of wastewaters containing non-biodegradable contaminants and producing extensive toxicity reduction. The Fenton process, which was developed by Henry Fenton in the 1890s, has gained increasing attention among AOPs. The advantages of the Fenton process are the need of a reagent easy to obtain, the flexibility of the operations, a short reaction time, and harmless by-products (Taylor et al., 2006). In addition, the Fenton process takes place at ambient temperature and barometric pressure. Below, Fenton process is analyzed in more detail and above all, photo-Fenton, which is the process used in this study.

4.1.1 Fenton and Photo-Fenton processes

In recent years, a remarkable effort has been made to better understand the Fenton process as a whole. The knowledge about the oxidation capabilities of the Fe²⁺/H₂O₂ combination (i.e. the Fenton-Reagent) is very old, and the mechanism has been known for some time (Bauer & Fallmann, 1997). The

highly reactive hydroxyl radicals and Fe^{2+} catalyst unselectively react with organic matter, concomitantly with the oxidation of Fe^{2+} into Fe^{3+} (Eq. (1)-(2)).

An interesting alternative to increasing the speed of this regeneration is to use a light source of a proper wavelength (photo-Fenton). The presence of UV-vis light allows reducing Fe^{3+} again into Fe^{2+} ($\lambda \leq 580$ nm), which in turn produces further $HO\cdot$ radicals (Eq.(3)) and results in a cycle continuously supplying $HO\cdot$ until H_2O_2 is depleted. Shorter wavelengths ($\lambda \leq 310$ nm) cause peroxide photolysis (Eq. (4)) and the direct production of extra $HO\cdot$. Therefore, the oxidation rate of photo-Fenton results much higher than that of the Fenton process.



The $HO\cdot$ radical is the key species that attacks organic compounds in a non-selective yet efficient way. However, if H_2O_2 is introduced in excess, an unduly high concentration of $HO\cdot$ might result in unproductive reactions (Eq. 5–6), lowering the efficiency of the process.



Among the AOPs, Fenton and photo-Fenton processes have received significant interest in the scientific community and many applications of both Fenton and photo-Fenton processes for the treatment of many kinds of wastewaters, can be found.

Regarding photo-Fenton process, efficient applications can be found mainly for the treatment of pharmaceuticals and pharmaceutical wastewaters (Jordá et al., 2011; Alam G. Trovó et al., 2012) and agrochemicals (Silva et al., 2012; Zhang & Pagilla, 2010). Moreover, photo-Fenton process also proved to be able to efficiently remove micropollutants (De la Cruz et al., 2013; Jung et al., 2012) and CECs as well (Miralles-Cuevas et al., 2014).

As a result, a significant experimental effort has been made in recent years to get a greater comprehension of the photo-Fenton process overall. The evaluation of important process efficiency characteristics was addressed in several studies conducted at both the laboratory and pilot plant scale.

Particularly, pH, Fenton reagents concentration, contaminant load and presence of other inorganic ions are some of the main factors affecting the photo-Fenton process efficiency (Rahim Pouran et al., 2015; Taylor et al., 2006; Zapata et al., 2010).

Regarding the pH influence, the range $2.5 < \text{pH} < 3.0\text{-}4.0$ ensures that the $\text{Fe}(\text{OH})^{2+}$ is present at appreciable concentration so allowing the reduction of Fe^{3+} to Fe^{2+} (Fenton-like reaction) at an appreciable rate (Pignatello, 1992; Taylor et al., 2006). Fenton reaction rates, on the other hand, tend to decrease above pH 3.0 due to catalyst precipitation.

Inorganic ions such as phosphate, sulphate, organosulfonate, fluoride, bromide, and chloride ions can inhibit the Fenton and photo-Fenton oxidations of organic compounds at variable levels depending on their concentrations. This inhibition could be due to catalyst precipitation, $\text{HO}\bullet$ scavenging, or the generation of a less reactive Fe^{3+} compound (Taylor et al., 2006).

Several researches have also shown the significance of H_2O_2 dosage (Audino et al., 2019; Santos-Juanes et al., 2011; Yamal-Turbay et al., 2015), in the improvement of the process performance, since it can avoid or reduce the activation of inefficient reactions scavenging hydroxyl radicals (Eq. (5)-(6)). The more efficient use of hydrogen peroxide allows for the reduction of operational costs, which are mostly attributable to oxidant and energy consumption. An excess of Fe^{2+} can scavenge hydroxyl radicals ($\text{Fe}^{2+} + \text{HO}\bullet \rightarrow \text{Fe}^{3+} + \text{OH}^-$) as well (Huston & Pignatello, 1999).

Furthermore, high oxidant concentrations are harmful to a wide range of microorganisms. This aspect must be considered while using conventional biological treatments in order to prevent microbial system damage.

Some works have finally shown the possibility of using easy measurable variables, e.g. dissolved oxygen (DO), hydrogen peroxide and TOC concentrations, as a way of developing further process monitoring and control applications (Cabrera-Reina et al., 2012). Changes in dissolved oxygen concentration have been linked to hydrogen peroxide decomposition: an increase in DO concentration indicates the activation of inefficient reactions that result in H_2O_2 decomposition, whereas a reduction in DO concentration indicates a shortage of hydrogen peroxide. As a result, Ortega-gómez et al., (2012) proposed using dissolved oxygen concentration data to design a process controller that ensures the proper and automatic dosage of hydrogen peroxide while limiting its consumption and maximizing the

pollutant mineralization rate. However, further research is needed in order to establish reliable and feasible oxidant dosing strategies.

Using H_2O_2 is essential, but oversupplying is counterproductive. The supply of hydrogen peroxide, as a means to control the concentration of hydroxyl radicals, is the most important operational parameter for the photo-Fenton process affecting both reaction outcome and process cost.

The mechanisms by which this oxidation occurs are complex, depend, of course, on the nature of organic molecules, and even in the case of simple molecules, can consist of many elemental reactions and many reaction intermediates. This is why these processes are often studied considering only the disappearance of the initial products (organic matter) and/or the generation of the final products (CO_2).

As a result, a number of studies have been conducted to determine the circumstances that would improve process performance through the use of a sensible hydrogen peroxide supply (Esteves et al., 2018; Rahim Pouran et al., 2015; Wang et al., 2016; Yamal-Turbay et al., 2015). The majority of proposals are heuristic approaches that are effective in specific situations, but a kinetic model would be the most appropriate solution that should be developed to provide the best solution.

Therefore, in order to treat the above-mentioned polluted waters, the contamination evolution should be predicted. It is then required to develop a model with a high level of accuracy (Audino et al., 2019). Although several aspects of the photo-Fenton process have been studied in the recent years, its mechanism and kinetic aspects are not yet fully understood. Not for lack of knowledge regarding the elementary reactions and equilibrium steps involved, but because a considerable number of intermediate radical species are generated during photo-Fenton and they are still under discussion.

On that account, special attention should be given to the design of the Photo-Fenton model in order to be able to study the working conditions of the system. Hence, in the following section an overview of possible modelling approaches is presented.

4.2 Mathematical modelling of chemical processes

Mathematical modelling is the process of describing a real world problem in mathematical terms, usually in the form of equations, and then using these equations both to help understanding the original problem, and also to discover new features about the problem.

Modelling is the necessary step to reduce and compact sensible experiences such as experimental data into abstractions useful for decision-making. The development of a practical model poses a trade-off

between its detail and complexity and its solvability, which is to be addressed in regard of the purpose and use of the model. The process modelling approaches can be mainly grouped in:

- First Principles Models (FPMs), based on physical theory;
- Data Based or Empirical Models (DBMs or EMs), strictly based on empirical descriptions;
- Semi-Empirical Models (SEMs), based on both physical theory and empirical descriptions.

4.2.1 Literature review of photo-Fenton processes modelling

First-principles modelling (FPM) is based on a complete and exhaustive understanding of the system e.g. mechanisms and material balances at the molecular level. It requires large amount of detailed data, which means measuring lots of system variables and solving large mathematically complex optimization problems for model fitting and parameter estimation. This is particularly true in the case of the complex chemistry of Fenton systems, whose details are now quite understood and reported elsewhere. Promising research into FPMs of photo-Fenton systems is underway, which include complex reaction mechanisms and design parameters as the light radiation, reactor shape, etc (Kušić et al., 2006; Ortiz de la Plata et al., 2010). Yet, current achievements are limited to pilot systems consisting of very few simple species such as formic acid, dichloroacetic acid or phenol.

However, FPMs, although desirable, may not be affordable. On one hand cost of developing and solving the corresponding mathematical models has to be considered, although computational power is expected to continue increasing and reducing its cost. On the other hand, it requires complex model fitting and parameter estimation, which in turn requires expensive analytical instrumentation allowing continuous monitoring of all the chemical species and conditions involved in the reaction.

As it has been mentioned, Fenton and photo-Fenton reactions are very complex; many elementary and many intermediate reactions are involved which are difficult to identify and measure. There are general mechanisms quite accepted (Eq. (1)-(2)), but depending on the organic compounds the particular mechanisms can be very diverse and unknown. However, to technically control this process, like any other, a model is needed that describes its evolution based on time and operating variables. If the system is too complex, it is necessary to select the elements of interest, it is necessary to make hypotheses and it is necessary to simplify. However, it is vital to be careful when be simplify or underestimate parts of the process, the most important thing is to be aware of the limitations of the model obtained.

In situations such as this one, the simplest option is to look only at the evolution of the concentration of the reagent of interest. In the case of a single organic compound, its concentration can be monitored. In more complex cases where there is a mixture of organic matter, aggregate parameters

such as TOC (Total Organic Carbon), COD (Chemical Oxygen Demand), or BOD (Biological Oxygen Demand) can be used, which do not consider the detail of the individual components.

Moreover, usual and cheaper measurement of lumped parameters such as TOC, COD, BOD, which show a global evolution of the system, does not allow inducing FPMs and cannot be considered satisfactory for this purpose. Therefore, when examining to which extent FPMs is practically affordable, the purpose of the model have to be taken into consideration.

On the opposite side, pure statistical modelling, instead, allows a practical and systematic approach to process characterization in terms of a response surface for regression models. The EMs have been very successful in determining response trends and variable interaction (Kušić et al., 2006; Pérez-Moya et al., 2008), and it has been proposed for practical black-box modelling in the area of Artificial Neural Networks (ANN) even for process control purposes (Göb et al., 2001). However, these modelling approaches are oversimplified cannot be used for extrapolation and process scale-up, as they do not provide information about the process dynamics. Furthermore, they have been shown to produce misleading conclusions regarding optimization.

Therefore, a semi-empirical model has been adopted for characterizing the performance of the process under study. On one hand, the degradation of the contaminant is measured through a lumped parameter such as the concentration of total organic carbon, [TOC], which allows a practical and inexpensive monitoring but provides a poor inference capacity in terms of fundamental explanation of the mechanism of the process. On the other hand, the model developed is intended for overcoming the limitations of pure statistical modelling and has been expressed in terms of physically meaningful factors that may be used for quantitatively assessing the performance of the process.

5 Photo-Fenton model

The photo-Fenton model that is used throughout this work is based on that by Cabrera-Reina et al. (2012) and later extended by Audino et al. (2019) and Nasr Esfahani et al., (2022) to include flexible H_2O_2 dosage and shedding new light on the dosage problem. Nasr Esfahani et al., (2022) work models a time-dependent supply of hydrogen peroxide to a batch reactor, and uses the experimental data obtained by Yu et al., (2020) using different dosage schemes for the mineralization of paracetamol solutions at a pilot plant scale. In this chapter, the exploited model in this project is thoroughly explained.

To simplify terminology, some nomenclature will be provided to refer to the work of each author:

- ACR, for Cabrera-Reina et al., (2012);
- FAU, for Audino et al., (2019);
- XYU, for Yu et al., (2020);
- KNE, for (Nasr Esfahani et al., 2022).

5.1 Kinetic and reactor model

Cabrera-Reina et al. (2012) proposed a set of simplified process reactions to create the model able to simulate TOC, hydrogen peroxide and oxygen evolution. The proposed model assumes eight states – these being the two ferric species (Fe^{2+} and Fe^{3+}); hydrogen peroxide (H_2O_2); the radicals formed from peroxide (whatever their form), R; the dissolved oxygen, DO; and three states accounting for the organic matter – two kinds of partially oxidized organics plus the parent compound present at the beginning of the reaction – named as MX_1 , MX_2 and M, respectively. These are the responsible for the measured lumped TOC parameter. The proposed reaction scheme is given in Figure 4. It is important to mention that, although the reactions below are numbered from equation 7 to 15, in Figure 4 they are numbered from 1 to 8, as indicated by the reaction rate and kinetic constants index in the equations.

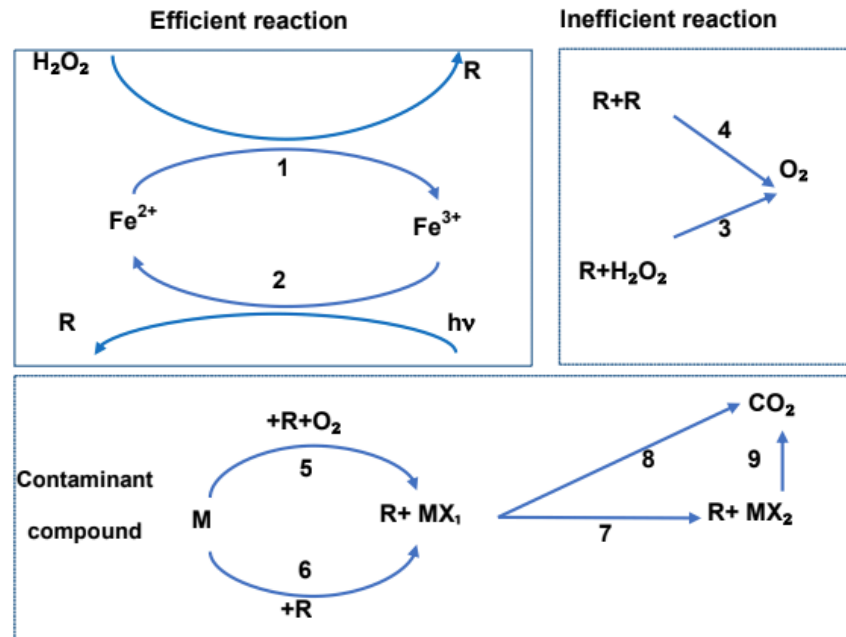


Figure 4: The reaction schematic of the photo-Fenton model according to Cabrera Reina et al. (2012). (Nasr Esfahani et al., 2022)

The formation of hydroxyl radicals is described through efficient reactions between Fe^{2+} and H_2O_2 (Eq.(7)) as well as Fe^{3+} and light (UV radiation) (Eq.(8)). The low pH requirement (between 3 and 6) is assumed, as usual, as an important condition for iron-induced reduction of hydrogen peroxide.

$$r_1 = k_1 \cdot [Fe^{2+}] \cdot [H_2O_2] \quad (7)$$

$$r_2 = k_2 \cdot [Fe^{3+}] \cdot [I] \quad (8)$$

The radicals formed in the first two reactions may have a useful pathway, reacting with organic matter; or may be lost in inefficient reactions with hydrogen peroxide; or lie between them leading to O_2 generation, which is reflected as a DO increase (Eq. (9)-(10)). Any of these reactions capacity to propagate is greatly dependent on the amount of hydrogen peroxide supplied as well as the rate constant. It's also worth mentioning that increasing hydrogen peroxide concentration reduces process efficiency by increasing radical concentration [R].

As Eq. (10) describes a second order reaction, its rate has an exponential shape. This leads to the existence of a low-concentration-zone at the beginning where this inefficient reaction takes place in a much lower peace. Later, on the contrary, the slope of the second order reaction becomes steeper and therefore inefficiency becomes more present. As a direct consequence, the importance of hydrogen peroxide dosage it is again evidenced.

$$r_3 = k_3 \cdot [R] \cdot [H_2O_2] \quad (9)$$

$$r_4 = k_4 \cdot [R] \cdot [R] \quad (10)$$

The remaining reactions are related to the oxidation of the main organic matter to produce MX_1 (Eq. (11)-(12)) and then MX_2 by means of Eq. (13). Finally, mineralization of the organics is modelled through Eq. (14)-(15).

$$r_5 = k_5 \cdot [M] \cdot [R] \cdot [O_2] \quad (11)$$

$$r_6 = k_6 \cdot [M] \cdot [R] \quad (12)$$

$$r_7 = k_7 \cdot [MX_1] \cdot [R] \quad (13)$$

$$r_8 = k_8 \cdot [MX_1] \cdot [R] \quad (14)$$

$$r_9 = k_9 \cdot [MX_2] \cdot [R] \quad (15)$$

The photo-Fenton degradation process dynamic model is based on mass balances for a batch operating mode of the relevant components in the model (Eq. (16)-(24)). They include the overall gas-liquid mass transfer coefficient for O_2 ($K_L a$) and the stoichiometric coefficients relating to the oxygen balance (c_1 , g_1 and g_2).

$$\frac{d[H_2O_2]}{dt} = \left(\frac{F}{V}\right) \cdot ([H_2O_2]_{in} - [H_2O_2]) - r_1 - r_3 \quad (16)$$

$$\frac{d[M]}{dt} = \left(\frac{F}{V}\right) \cdot ([M]_{in} - [M]) - r_5 - r_6 \quad (17)$$

$$\frac{d[MX_1]}{dt} = \left(\frac{F}{V}\right) \cdot ([MX_1]_{in} - [MX_1]) + r_5 + r_6 - r_7 - r_8 \quad (18)$$

$$\frac{d[MX_2]}{dt} = \left(\frac{F}{V}\right) \cdot ([MX_2]_{in} - [MX_2]) + r_7 - r_9 \quad (19)$$

$$\frac{d[TOC]}{dt} = \frac{d[M]}{dt} + \frac{d[MX_1]}{dt} + \frac{d[MX_2]}{dt} \quad (20)$$

$$\frac{d[O_2]}{dt} = \left(\frac{F}{V}\right) \cdot ([O_2]_{in} - [O_2]) + g_1 r_3 + g_2 r_4 - c_1 r_5 + (K_L a ([O_2]^* - [O_2])) \quad (21)$$

$$\frac{d[Fe^{2+}]}{dt} = \left(\frac{F}{V}\right) \cdot ([Fe^{2+}]_{in} - [Fe^{2+}]) - r_1 + r_2 \quad (22)$$

$$\frac{d[Fe^{3+}]}{dt} = \left(\frac{F}{V}\right) \cdot ([Fe^{3+}]_{in} - [Fe^{3+}]) + r_1 - r_2 \quad (23)$$

$$\frac{d[R]}{dt} = \left(\frac{F}{V}\right) \cdot ([R]_{in} - [R]) + r_1 + r_2 - r_3 - 2r_4 - r_5 - r_6 - r_7 - r_8 - r_9 \quad (24)$$

Where F represents the inlet flow-rate ($L \cdot h^{-1}$) that produces a variation in the total volume of the reactor V (L), while $[C_i]_{in}$ as well as $[C_i]$ refer to the concentrations ($mmol \cdot L^{-1}$) for each element in the inlet flow rate and inside the reactor, respectively. Because the study primarily looks at hydrogen peroxide dosage, only the $[H_2O_2]_{in}$ differs from zero, and the rest of the inlet concentrations are null.

Finally $[DO]^*$ represents the dissolved oxygen saturation concentration, and $[DO]_0$ represents the initial dissolved oxygen concentration, both expressed as $mmol \cdot L^{-1}$.

Hence, the model parameters of Cabrera-Reina et al., (2012) photo-Fenton model to be considered are: k_1 to k_9 , $K_L a$, and stoichiometric coefficients c_1 , g_1 and g_2 .

Furthermore, for the sake of simplicity, nomenclature is completed with the following terms:

- Generic reaction time t , and final time τ for the reaction (and the ODEs integration), at which the reaction performance is evaluated;
- Conversion, $\chi(t)$ and $\chi(\tau)$, which is defined by Equation (25) and assesses the relative ratio of TOC removal at a given time:

$$\chi(t) = ([TOC]_0 - [TOC]_t) / [TOC]_0 \quad (25)$$

- $A(t)$, $A(\tau)$, which is described by Equation (26) and analyses the entire expenditure of H_2O_2 in the batch run, given by the initial amount and the dosed amount:

$$A(t) = A_0 + C \int_0^t F(t) dt \quad (mmol) \quad (26)$$

The following assumptions underpin the model (Audino et al., 2019):

- Because the reaction between Fe^{3+} and H_2O_2 is ignored, the model can only be applied to the photo-Fenton process (UV light is required);
- The different radical species that may exist are represented by their aggregated concentration $[R]$ and common behavior;

- III. Hydrolysis of H_2O_2 is ignored;
- IV. It is assumed that an intermediate oxidized compound exists before any CO_2 released from the process.

The model used in this project include a focus on easy-to-monitor parameters like hydrogen peroxide, dissolved oxygen, and TOC; the use of unspecified intermediates (MX_1 , MX_2 , as artificial, dummy variables) to model the delay in the response of this practical lumped measurement; and the simple modelling of H_2O_2 scavenging via non-linear radical consumption (Eq. (9)-(10)). In other words:

- The organic matter is firstly degraded and then mineralized. Thus, the delay is modelled with organic matter intermediates;
- Even the initial organic contaminant is PCT, the monitored substance is TOC, because of its simplicity;
- As the radical consumption is a second order reaction, the H_2O_2 dosage can be modelled while trying to dose within the low reaction speed zone.

Accordingly, Nasr Esfahani et al., (2022) accepted the above equations (Eq. (7)-(24)) and model parameters as initial values and adapted them to a series of pilot-plant experiments by conducting model global sensitivity analysis (GSA) and parameter estimation using Simulink®.

In the following two sections, the experimental data and the adaptations made by Nasr Esfahani et al., (2022) (e.g. GSA and parameter estimation) will be briefly explained. The only purpose of this is to make the understanding of the implemented model more clear.

5.2 Reference data

Yu et al., (2020), which addresses the formulation of the optimization of a fully flexible H_2O_2 dosage profile in photo-Fenton processes and its experimental solution, also provided the experimental data used to calibrate the model. The work is limited due to the hefty cost of conducting experiments, but it emphasizes the need for a reliable process model and provides data for calibrating one.

Yu et al. (2020) evaluated the photo-Fenton remediation of PCT, and the experimental results included the evolution of TOC, H_2O_2 , and DO concentrations. The data supplied refers to a set of systematically designed dosage profiles that cover the entire range of alternatives (Table 1). The reaction time (2h) was divided into eight time slots of 15 minutes (S1 to S8), with each dosage set active or not (1, 0) to ensure that the same amount of H_2O_2 was fractioned and distributed throughout the time period.

The first slot (S1) was obviously always on (1) for all profiles, while the last three (S6, S7, and S8) were decided to be off (0). As a result, there were four degrees of freedom (S2, S3, S4, and S5) and 16 cases that lead to the codification in Table 1. The label no dosage denotes an assay in which the same total amount of H₂O₂ was supplied all at once at the start, and for which this codification does not apply (N/A).

It is worth mentioning that the dosage profiles of the simulations performed during the model exploitation in the present project were also based in Yu et al., (2020) experiment design.

Table 1: XYU design experiments (Yu et al., 2020).

ID (code)	ID (bin)	S1	S2	S3	S4	S5	S6	S7	S8	Fraction per slot
No dosage	N/A	N/A	N/A	N/A	N/A	N/A	N/A	N/A	N/A	N/A
0	0000	1	0	0	0	0	0	0	0	1
1	0001	1	0	0	0	1	0	0	0	1/2
2	0010	1	0	0	1	0	0	0	0	1/2
3	0011	1	0	0	1	1	0	0	0	1/3
4	0100	1	0	1	0	0	0	0	0	1/2
5	0101	1	0	1	0	1	0	0	0	1/3
6	0110	1	0	1	1	0	0	0	0	1/3
7	0111	1	0	1	1	1	0	0	0	1/4
8	1000	1	1	0	0	0	0	0	0	1/2
9	1001	1	1	0	0	1	0	0	0	1/3
10	1010	1	1	0	1	0	0	0	0	1/3
11	1011	1	1	0	1	1	0	0	0	1/4
12	1100	1	1	1	0	0	0	0	0	1/3
13	1101	1	1	1	0	1	0	0	0	1/4
14	1110	1	1	1	1	0	0	0	0	1/4
15	1111	1	1	1	1	1	0	0	0	1/5

Fourteen of the sixteen experiments detailed in Table 1 were used by Nasr Esfahani et al., (2022) to calibrate the model (e.g. parameter estimation). Although prior to that, he undertook the global sensitivity analysis.

5.3 Global sensitivity analysis (GSA) and parameter estimation

GSA was carried out by Nasr Esfahani et al., (2022) to assess to which extent variations of the model parameters affect each measured response (H₂O₂, TOC, and DO – the experimentally available data). Two of the reactions proposed were found to have scarce influence on the fitting of the model. This resulted in the rejection of two reactions of the initial model. Concretely, reactions 12 and 14, meaning that k_6 and k_8 have null value. Therefore, the kinetic constants (k_1 , k_2 , k_3 , k_4 , k_5 , k_7 , k_9 , $K_{1,a}$), stoichiometric coefficients c_1 , g_1 , and g_2 , in addition to operational parameter I , were finally the 12 parameters to be estimated.

With reference to parameter estimation, there is a challenge when trying to fit a non-linear model to experimental data, and is the initial estimation of the parameters. If fitting methods converge, they may find distinct sets of parameter values or converge to local solutions. Nasr Esfahani et al., (2022) employed an approach detailed elsewhere to perform the estimation.

Table 2 shows the initial values provided by Cabrera-Reina et al., (2012), which were used by Esfahani et al., (2022) as initial guesses as well as the fitted values. The present work uses KNE fitted ones.

Table 2: Initial model parameter from Cabrera-Reina et al., (2012) and fitted parameters from Esfahani et al., (2022) used in the present work.

Kinetic constants	ACR Initial value	KNE Fitted value
I (W. m⁻²)	32	31.92
K_La (h⁻¹)	2.7	0.499
c₁	0.1	6.011
g₁	0.75	0.472
g₂	0.47	0.631
k₁ (mM⁻¹.h⁻¹)	8.81	9.022
k₂ ((W. m²)⁻¹.h⁻¹)	5.63	32.237
k₃ (mM⁻¹.h⁻¹)	75.8	2.335
k₄ (mM⁻¹.h⁻¹)	42,798	45,585
k₅ (mM⁻¹.h⁻¹)	2,643	1,099.7
k₆ (mM⁻¹.h⁻¹)	257	0
k₇ (mM⁻¹.h⁻¹)	2,865	45,644
k₈ (mM⁻¹.h⁻¹)	271	0
k₉ (mM⁻¹.h⁻¹)	107	91.136

5.4 Mathematical tools

The model, which is given by the set of Ordinary Differential Equations (ODEs) (Eq. (16) to (24)), was implemented by Nasr Esfahani et al., (2022) in MATLAB/Simulink® version R2021b and numerically solved using the ode15s solver as a variable order solver based on numerical differentiation formulas with a time variable-step.

The validation using fitted values with different dosage profiles confirmed the capacity of the model to accurately explain alternative dosage schemes, showing acceptable average errors. It confirmed that the model representation of the system under investigation was adequate. The model and adjustment

procedure demonstrated that they were capable of reproducing the evolution of the reaction under a variety of dosage schemes and predicting future situations under new operating conditions.

As a result, the tools and methodological approach are ready to test and evaluate other dosage strategies that could be designed, as will be done in the current study. The systematic examination of alternatives may eventually lead to the identification of the best dosage strategy for each situation.

5.4.1 Simulation methodology

Thanks to the model implemented by Nasr Esfahani et al., (2022) in Simulink®, it was possible to modify all the variables of the system. However, due to time constraints, not all of them were modified in this project. Figure 5 shows the simplified structure of the Simulink® model used. It basically comprises the input variables, which are introduced in the reactor block containing the ordinary differential equations, where they are solved to obtain the output results. The total volume of the reactor is 15 L.

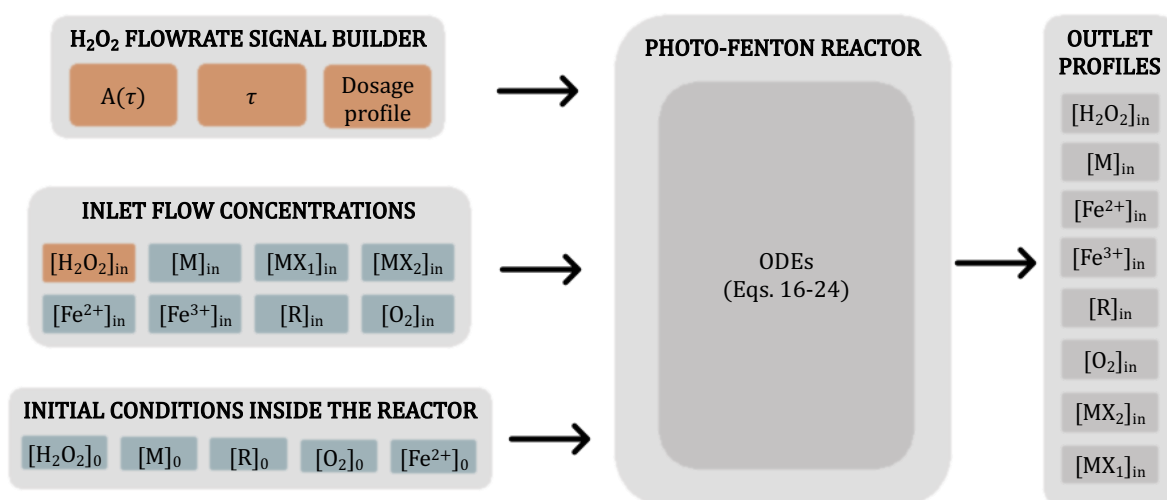


Figure 5: Simplified scheme of Simulink® model. Variables (orange), parameters (blue).

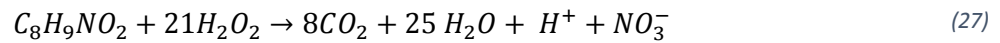
In this project, the decision variables were those highlighted in orange in Figure 5, such as total amount of hydrogen peroxide ($A(\tau)$), processing time (τ), the hydrogen peroxide dosage profile and, consequently, the concentration of hydrogen peroxide in the inlet flow $[H_2O_2]_{in}$.

On the other hand, the initial conditions inside the reactor such as the concentration of catalyst $[Fe^{2+}]_0$, the amount of light $[I]$, concentration of oxygen $[O_2]_0$ or the concentration of pollutant $[M]_0$ were kept constant and, as mentioned above, the concentrations of all components of the input stream will have a value equal to zero except for the concentration of hydrogen peroxide, which is considered as a variable. These constant parameters are highlighted in blue in Figure 5 and its values are shown in Table 3:

Table 3: Fixed variables in the simulations.

Concentration	Value	Concentration	Value
$[H_2O_2]_0$ (mM)	0	$[MX_1]_{in}$ (mM)	0
$[M]_0$ (mM)	0.26	$[MX_2]_{in}$ (mM)	0
$[O_2]_0$ (mM)	0.64	$[R]_{in}$ (mM)	0
$[Fe^{2+}]_0$ (mM)	0.179	$[O_2]_{in}$ (mM)	0
$[R]_0$ (mM)	0	$[M]_{in}$ (mM)	0
$[Fe^{2+}]_{in}$ (mM)	0	$[Fe^{3+}]_{in}$ (mM)	0

The concentration of the pollutant (i.e. PCT) is the same in all simulations. Thus, the stoichiometric value of hydrogen peroxide ion concentration to achieve total mineralization of 0.2646 mmol L⁻¹ of PCT, when H₂O₂ is considered to be the only oxidant in the media, is 5.56 mmol L⁻¹ (Equation (27)).



In order to calculate $[H_2O_2]_{in}$ (mmol L⁻¹), in both dosage experiments a 30% v/w hydrogen peroxide solution was used, which corresponds to 8823 mmol L⁻¹.

Since Yu et al., (2020) employed this quantity of 5.56 mmol L⁻¹ in all of her tests, in the present work it was used as the reference amount (S). Its effect on the system will be explored by changing its value.

In reference to the decision variables, some clarifications in reference to how they were modified are:

- The total hydrogen peroxide quantity $A(\tau)$ applied in the simulations was always a proportional value to the reference value (S) (i.e. 5.56 mmol L⁻¹) (e.g. S, 2S, 3S, etc.).
- The processing simulation durations (τ) under study range from 0 to 30 hours.
- To build the dosage profile, the processing time was divided into 15-minute time slots (S₁ to S_n), with each dosage set active or inactive (1, 0) to ensure that the same amount of H₂O₂ was fractioned and distributed throughout the time period.

The final problem was to find both the hydrogen peroxide addition profile and the reaction time τ that maximized the overall performance of photo-Fenton treatment.

To accomplish this, the model was first tested by evaluating the calculated KNE parameters and by reproducing some of the experiments used to fit the model. Then, the effect of each of the decision

variables in the system was studied to finally find with the goal of determining high-performance dosing configurations based on the model (see Figure 2).

After exploiting the model now presented and reaching certain conclusions thanks to the simulations, it was then necessary to validate the hypotheses that have been formulated. For this reason, it was required to take them to the pilot plant to verify the veracity of the model prediction.

6 Experimental methods

This chapter provides an overview of the experimental settings and analytical methods that were used to collect data that contributed to a better understanding of the AOPs under research.

6.1 Experimental setting

This section provides an overview of the pilot plant that was used to conduct photo-Fenton experiments, serving as the case study of the thesis. The CEPIMA (Center for Process and Environmental Engineering, Universitat Politècnica de Catalunya, Barcelona, Spain) designed this pilot plant.

Finally, the experimental section is tangled up with a presentation of the materials, with a special emphasis on the target compounds that were used to carry out the required experiments. The final section includes a description of the applied analytical techniques as well as the design of experiment technique.

6.1.1 Fenton/Photo Fenton pilot-plant

The system consists of a 15.0-L glass jacketed tank that can serve as both a reservoir and a photoreactor because it has an axially located lamp holder, and a glass annular reactor that also has an axially located lamp holder. These two reactors can be used separately or in tandem. The pilot plant configuration chosen for this study was one with a glass jacketed tank as the reservoir and a glass annular reactor as the photoreactor.

The UVA-UVB radiation source was a Philips Actinic BL TL-DK 36 W/10 1SL lamp (UVA-UVB). Figure 6 shows the spectrum of the lamp when viewed through a Pyrex envelope.

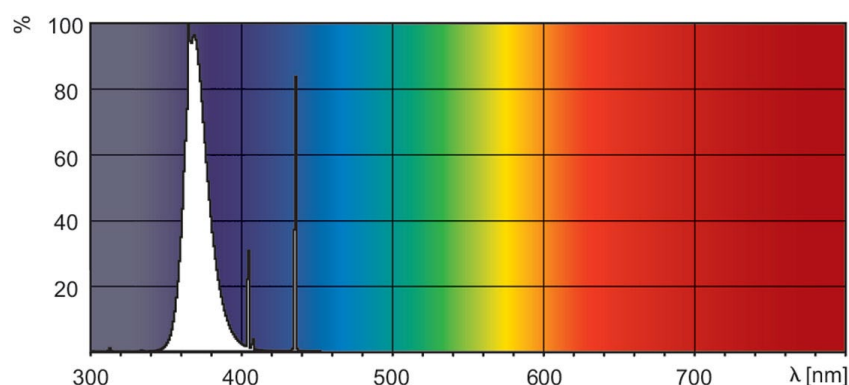


Figure 6: Spectrum of a Philips Actinic BL TL-DK 36 W/10 1sl lamp. (Philips, 2022)

Figure 7 shows a photograph of the glass annular photoreactor, together with its parameters and lamp characteristics.


REACTOR	CHARACTERISTICS
	Irradiated volume: 1.5 L
	Irradiated height: 130.0 mm
	Outer cylinder: Outer diameter: 150.0 mm
	Outer cylinder: Inner diameter: 130.0 mm
	Inner cylinder: Outer diameter: 70.0 mm Inner cylinder: Inner diameter: 63.6 mm
	IRRADIATION SYSTEM
	Lamp: Philips Actinic BL TL-DK 36 W/10 1SL lamp (UVA-UVB): (diameter: 28.0 mm, length: 589.8 mm)

Figure 7: Annular photoreactor characteristics and irradiation system.

Figure 8 shows a schematic representation of the pilot plant with the various components that will be discussed further on.

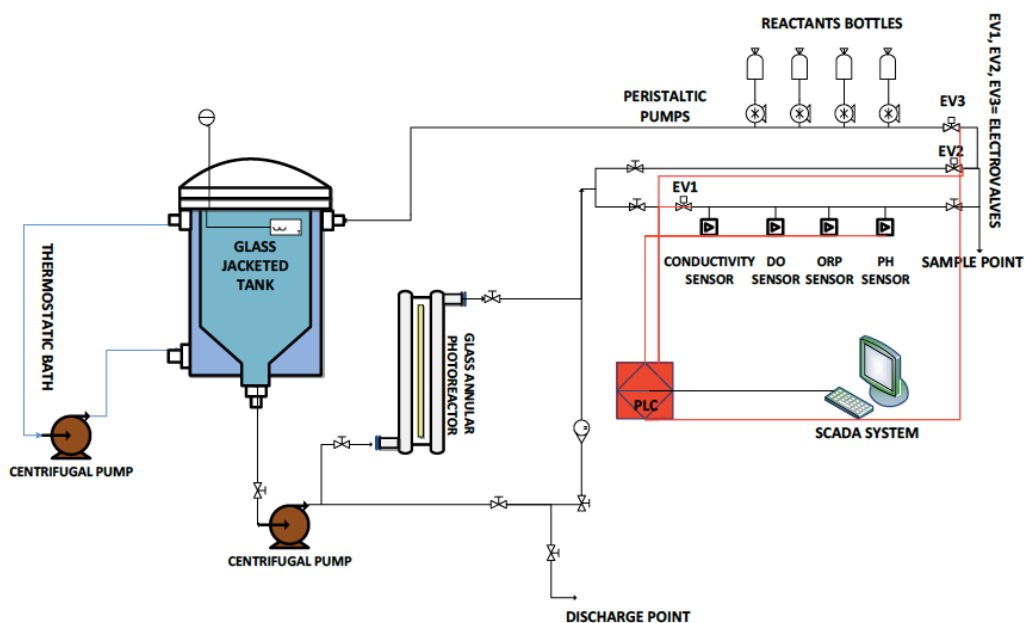


Figure 8: Schematic view of the pilot-plant. (Audino, 2019)

A centrifugal pump (Iwaki Magnet Pump, MD- 30RZ-220, 1-16HP-220V) is coupled to a variable frequency inverter (Eurotherm, CFW-10 series) that permits adjusting the flowrate from 2.0 to 15.0 L min⁻¹ to assure operating under optimal mixing circumstances.

A rotameter (Tecfluid 6001/PVC ¾") is used to monitor the recirculation flowrate via the system. In addition, four peristaltic pumps (Watson Marlow, OEM 313 24V) are equipped for possible reactant dosage. Two electro valves (Hunter PGV-101G-B 1"), labelled EV2 and EV3 in Figure 8, are situated before pumping line of the peristaltic pumps.

A measurement line is also installed in the pilot plant, including sensors for pH, dissolved oxygen, conductivity, and oxidation-reduction potential (ORP).

A proportional electro-valve (mPm L20 - J2), labelled EV1 in Figure 8, maintains a flowrate of 1.0 mL min⁻¹ across this measurement line. The recirculation flowrate may be measured through this measuring line using a flowmeter (DIGMESA 04 – 16 L min⁻¹, 800 p/L) linked to a Eurotherm 2132i indication (4 – 16 L min⁻¹).

A UV sensor probe (sglux UV Surface A 4-20mA cable) is also mounted on the annular exterior surface of the photoreactor for surface measurements with a sensitivity range of 1 nW cm². UV rays may be measured and collected in real time (every second) with this sensor.

Finally, within the tank reactor is a temperature probe PT-100 that is coupled to a Eurotherm 2132i indication. It's worth noting that the temperature of the system can be kept consistent owing to a thermostatic bath.

The pilot plant is equipped with a Programmable Logic Controller (PLC) connected to Wonderware® InTouch® software, which allows data acquisition from in/out modules connected to the installation (e.g. sensors) and data management from an OPC (OLE for Process Control) server throughout a SCADA (Supervisory Control And Data Acquisition) system with the goal of allowing process control.

The ability to set the dose of the Fenton reactants (H_2O_2 , $\text{Fe}^{2+}/\text{Fe}^{3+}$) is one of the benefits of connecting to a PLC-SCADA system. A stepwise dosing strategy is implemented using InTouch® software and a PID (Proportional–Integral–Derivative) that needs the definition of the quantity of reactant to be dosed over a certain time period.

6.1.2 Reagents and chemicals

Because it is one of the top 200 medications prescribed worldwide and is commonly used as an antipyretic and analgesic, paracetamol (PCT) was chosen as a pollutant to design the model.

PCT is continually discharged through hospital waste, as well as consumer usage and disposal (Langford & Thomas, 2009). According to Muir et al., (1997), PCT is excreted in 58-68% during therapeutic treatment. As a result, it has been found in sewage treatment plant effluents in the g L^{-1} range (Ternes, 1998), in natural water sources, such as the Tyne River (UK), and even in groundwater at concentrations ranging from g L^{-1} to ng L^{-1} (Antunes et al., 2013).

Finally, the use of paracetamol as a model contaminant must be recognized as a reasonable and well-documented method for producing recalcitrant synthetic wastewater (Alam Gustavo Trovó et al., 2008). PCT was also chosen because of its molecular simplicity and low biodegradability, making it ideal for both experimental and modelling tasks.

In addition, more reagents were used for the photo-Fenton experiments: hydrogen peroxide, heptahydrate ferrous sulphate ($\text{FeSO}_4 \cdot 7\text{H}_2\text{O}$) as the ferrous ion, ammonium metavanadate (NH_4VO_3 98.5%) used for H_2O_2 measurement and sulfuric acid (H_2SO_4 95%) to control the pH. All chemical compounds used are summarized in Table 4.

Table 4: Chemical compounds used in the experiment.

Name	Formula	Molecular weight (g mol ⁻¹)	Purity (%)	Provider
Paracetamol	C ₈ H ₉ NO ₂	151.17	98	Sigma-Aldrich
Hydrogen peroxide	H ₂ O ₂	34.01	30 (w/v)	Panreac
Heptahydrate ferrous sulphate	FeSO ₄ ·7H ₂ O	278.01	100	Merck
Ammonium metavanadate	NH ₄ VO ₃	116.98	98.5	Fisher
Sulfuric acid	H ₂ SO ₄	98.08	95	Fisher

6.2 Analytical techniques

This section contains a description of the analytical procedures and equipment utilized in this study to describe the performance of the AOPs under investigation.

In particular, Total Organic Carbon (TOC) and model pollutant concentrations were measured in photo-Fenton studies. Furthermore, the concentration of the Fenton reagent H₂O₂ was measured using a spectrophotometric approach during the experiments.

6.2.1 Total Organic Carbon (TOC) determination

The quantity of carbon in an organic substance is represented by the Total Organic Carbon (TOC). It's a single parameter that provides an indirect measurement of all organic components in a water sample.

Because it is nearly hard to detect and track the deterioration of each intermediate generated during the treatment, the TOC is of great interest. As a result, the TOC is used to assess the mineralization of organic matter in a water sample, or as a water quality indicator. TOC is calculated by evaluating Total Carbon (TC) and Total Inorganic Carbon (TIC), with the difference between the two resulting in TOC.

The TC analysis is based on the combustion of an aqueous sample in a tube filled with platinum catalyst on an aluminum spheres support heated to 680.0°C. The carbon in the sample is thus oxidized to CO₂. The CO₂ is then swept onto a dehumidifier, where it is chilled and dried, using a CO₂ free carrier gas (purified air) flowing at a predetermined flowrate (150.0 mL min⁻¹). Finally, the CO₂ reaches a non-dispersive infrared (NDIR) detector, which examines the signal created by the CO₂ absorbance, which

is then analyzed by the software of the equipment. The area of the peak produced by the NDIR detector signal is proportional to the concentration of TC.

Total inorganic carbon (TIC) is measured in a reaction chamber by mixing the sample with a 25% w/v phosphoric acid (H_3PO_4) solution. The acidified sample is subsequently sparged with free carrier gas to achieve carbonate and bicarbonate degradation into CO_2 , which is then dehumidified and analyzed using a NDIR detector and evaluated using the equipment's software. A linear relationship between peak area and carbon content (for TC and TIC) is produced by preparing standard solutions in ultra-pure water (Milli-Q® system) for measurement.

The TOC analysis in this study was performed on a Shimadzu TOC-VCSH/CSN analyzer (Shimadzu; Kyoto, Japan).

Because of the time constraints (each measurement lasts 15.0 minutes), samples were taken every 15.0 minutes and refrigerated after extraction to prevent additional deterioration of the organic materials.

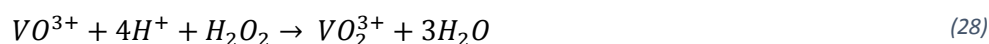
The TC measurement was calibrated using potassium hydrogen phthalate standard solutions, while the TIC measurement was calibrated using sodium carbonate/sodium hydrogen carbonate standards, according to the calibration curves.

6.2.2 Hydrogen peroxide determination via spectrophotometric technique

Hydrogen peroxide is the oxidant used in the Fenton and photo-Fenton water treatment processes. The efficacy of chemical oxidation of organic matter can be evaluated by measuring the residual concentration of hydrogen peroxide and, as a result, its consumption during the treatment period. It's also possible to draw inferences about how much hydrogen peroxide is needed to achieve the required mineralization level and/or predict contaminant degradation.

There are several ways for determining hydrogen peroxide, however this study used the spectrophotometric approach proposed by Nogueira et al., (2005), which has the advantages of being cost-effective and fast.

The methodology is based on the measurement of the peroxovanadium cation (VO_2^{3+}) absorbance at 450 nm, which results from the interaction of hydrogen peroxide with ammonium metavanadate in an acidic medium:



To ensure that all of the hydrogen peroxide interacts with the ammonium metavanadate, an excess of ammonium vanadate was always added. According to the stoichiometry of the reaction in Eq. (28), the final concentration of peroxovanadium is equal to the starting concentration of hydrogen peroxide. Because the absorption at 450 nm is proportional to $[\text{VO}_3]$, it can be measured using UV-visible spectrophotometry.

During photo-Fenton studies, a Hitachi U-2001 UV-VIS spectrophotometer (Tokyo, Japan) was used to measure hydrogen peroxide concentrations. Until the end of the treatment, samples were collected every 15.0 minutes.

6.3 Pilot-plant experiments

As first instance, an experiment previously performed by Yu et al., (2020) was carried out in order to check that the operation of the pilot plant was the same as when she used it to perform her experiments. Particularly, experiment 1111 was the one successfully performed, defined elsewhere.

Then, a set of two experiments using paracetamol (PCT $\text{C}_8\text{H}_9\text{NO}_2$) as target compound were carried out to test the validity of selected scenarios from the simulations.

Particularly, the photo-Fenton experiments were performed using the same initial concentrations of the simulations. The initial solution in the reactor was prepared with 15 L of distilled water and 0.6122 g of model pollutant PCT and 0.7468 g of $\text{FeSO}_4 \cdot 7\text{H}_2\text{O}$ (40 mg L^{-1} PCT and 10 mg L^{-1} Fe^{2+} or 0.2646 mmol PCT and 0.179 mmol Fe^{2+}).

The conditions of the photo-Fenton experiments were: pH adjusted to 2.8 ± 0.2 using H_2SO_4 and temperature 26–28°C.

In consequence of the simulation results, two high-performance scenarios (see Table 5), were investigated.

Table 5: Experiments performed in pilot-plant scale.

ID	$[\text{H}_2\text{O}_2]_{\text{in}}$ (mM)	$[\text{M}]_0 = [\text{TOC}]_0$ (mM)	$[\text{Fe}^{2+}]_0$ (mM)	Dosing time (min)	τ (min)
EXP1	5.56	0.26	0.179	60	120
EXP2	16.68	0.26	0.179	240	300

In the first experiment (EXP1) the total amount of hydrogen peroxide added was three times the reference amount S. Therefore, being 28.35 mL of solution, which corresponds to 567 mg L^{-1} . In this

case, 2 hours was the process time (τ), using the first one to dose constantly all 28.35 mL of H_2O_2 solution and the last one with no dosage. (Figure 9a).

On the other hand, in second experiment (EXP2) the total amount of hydrogen peroxide to be dosed, A , was set to be the stoichiometric concentration (considering H_2O_2 as the only oxidant in the media), S , for the given amount of PCT: this is 9.545 g (9.45 mL H_2O_2 of solution 30%w/v), which corresponded to a concentration of 189 mg L^{-1} (S). The process time (τ) was 5 hours, where the first 4 hours were used to dose the 9.45 mL of solution constantly and the last hour without dosing. (Figure 9b).

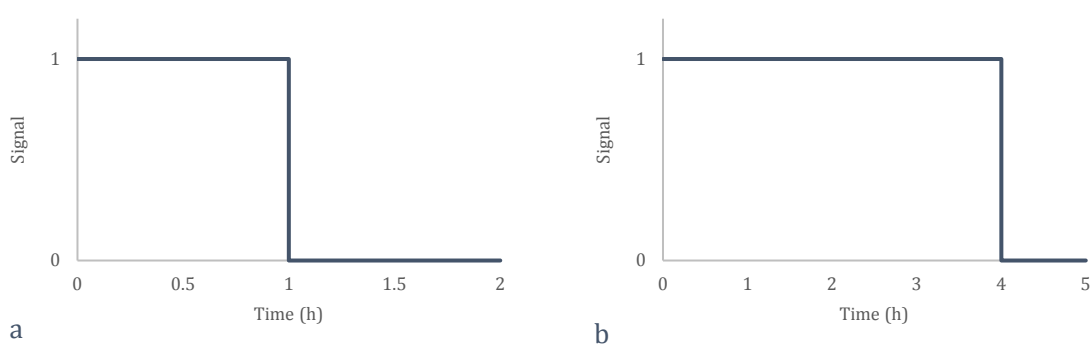


Figure 9: H_2O_2 flowrate signal: a) EXP1; b) EXP2.

7 Results and discussion

Different sets of simulations were planned to assess the performance of the dosing strategy for a water contaminated with paracetamol (Table 6). This concentration was kept constant at 40 mg L⁻¹ in all simulations.

The assays were discussed in terms of several outcomes, such as the evolution of the TOC concentration, and were quantitatively evaluated in terms of how hydrogen peroxide was used to achieve mineralization of the organic load. Another performance indicator considered in this work was the oxygen concentration in solution during the experiments, which should ideally be kept in a low range to minimize side reactions.

Table 6: Executed simulations.

Simulation	Section	Aim	Figure related
1	Preliminary simulation results	Check the adjustment of KNE parameters	Figures 10, 11, 12
2		Check the predictive ability of the model for all variables	Figures 13, 14
3	Model exploitation results and discussion	Examine the effect of τ and $A(\tau)$ in XYU experiments	Figures 15, 16, 17
4		Dosing hydrogen peroxide more efficiently	Figure 18
5		Evaluate the effect of different random dosage profiles	Figure 19
6		Achieve 100% mineralization	Figure 20

7.1 Preliminary simulation results

Preliminary simulations were conducted in order to study the behavior of the system and verify the goodness of the predictions of the model. ACR and KNE parameters were used to simulate the sixteen experiments designed by Yu et al., (2020) (Table 1). The purpose was to investigate the system response while using the initial parameters and the fitted. Result analysis was based on the final TOC removal, $\chi(\tau)$, for a fixed reaction time $\tau = 2$ h (Table 7).

Table 7: $\chi(\tau)$ results for XYU experiments and ACR and KNE simulations.

ID (code)	ID (bin)	$\chi(\tau)$		
		XYU (experimental)	ACR parameters (simulation)	KNE parameters (simulation)
0	0000	61,70	67,23	62,52
1	0001	55,50	68,89	60,11
2	0010	60,55	69,25	61,33
3	0011	56,95	68,21	58,53
4	0100	60,35	68,76	61,84
5	0101	58,15	68,90	60,08
6	0110	57,39	68,59	60,43
7	0111	57,40	67,98	58,62
8	1000	61,90	67,70	62,01
9	1001	57,70	69,07	61,17
10	1010	58,40	68,90	61,50
11	1011	57,85	68,67	59,84
12	1100	59,20	68,17	61,51
13	1101	57,43	68,70	60,54
14	1110	57,50	68,36	60,66
15	1111	58,45	68,30	59,61
No dosage	N/A	57,15	73,38	62,35

The ACR and KNE results were compared with those of XYU by measuring the $\chi(\tau)$ difference of the simulation (i.e. ACR or KNE $\chi(\tau)$) with the experimental value of XYU). Figure 10 illustrates the different mineralizations between the simulations and the experimental values. The results, as expected, show better agreement with the adjusted KNE parameters, as the differences are smaller in all cases. When using the ACR parameters, differences between the results with the experimental XYU values range from 5 to 16 units, but using the KNE parameters, the differences are at most 5.

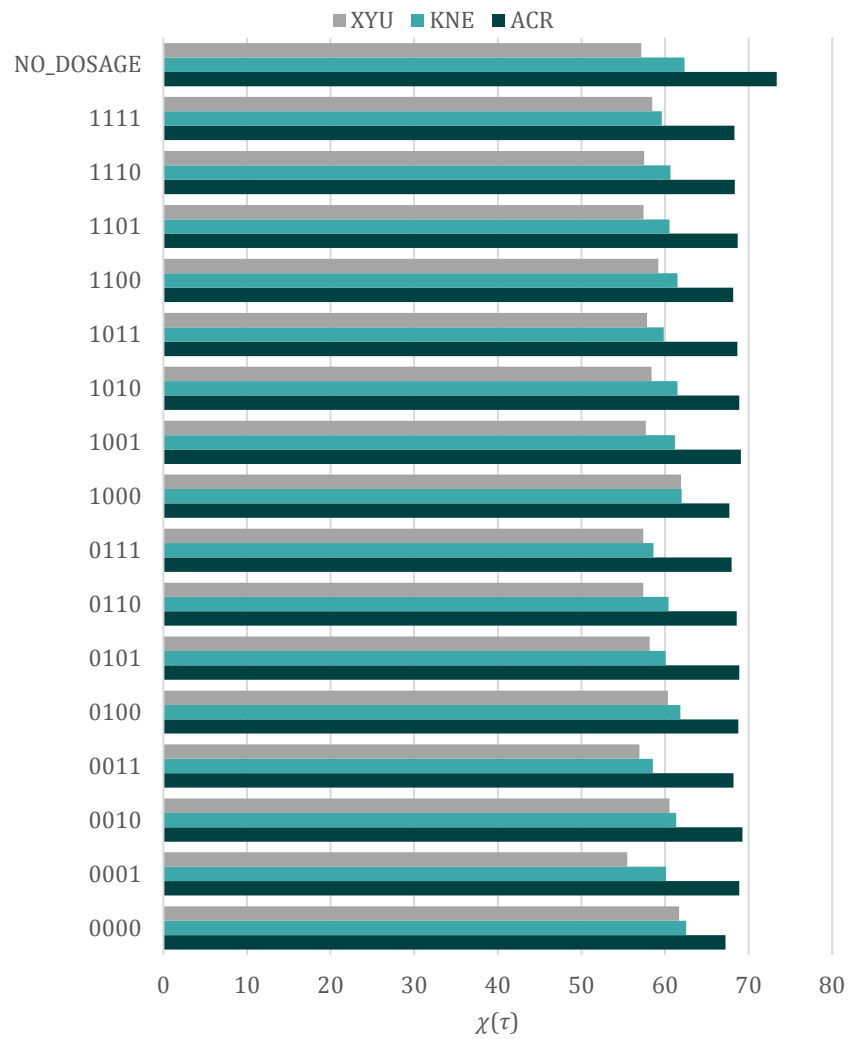


Figure 10: $\chi(\tau)$ differences between experimental (XYU) and simulation (ACR and KNE) results.

In spite of their variability, the average KNE values estimated for the model parameters are adequate for producing the practical model results that match the experimental results (Figure 11 and Figure 12). Figure 11 and Figure 12 compare the experimental and simulated data with the ACR and KNE parameters of two cases: 0010 and 1101 given in Table 1. 0010 is defined by an active input flow rate from 0 to 15 min and from 45 to 60 min and 1101 by an active input flow rate from 0 to 45 min and from 60 to 75 min.

The results show the evolution of TOC, H_2O_2 and oxygen from the two experiments to check the fit of the simulation to the data. The image shows the ability of the model to reproduce the measured behaviour of the process, notably the changing trend of H_2O_2 or DO profiles.

As expected, the results indicate a better fit when using KNE parameters, especially when measuring oxygen evolution. This is in line with the results reported by Cabrera-Reina et al., (2012), who reported that his model predicts TOC and H_2O_2 evolution accurately, but not oxygen.

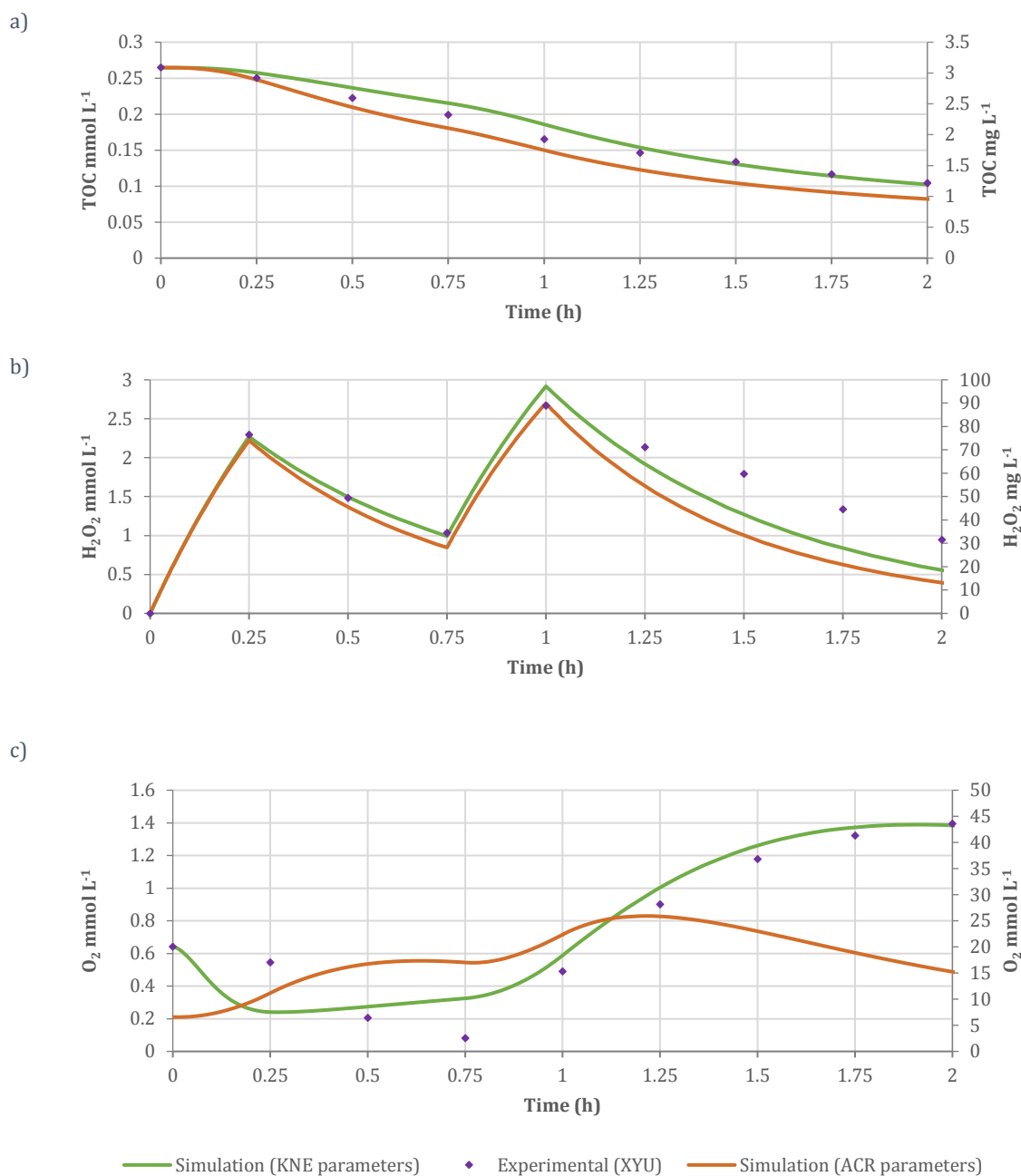


Figure 11: Experimental data (XYU) and predicted profiles (ACR and KNE) in 0010 dosage.

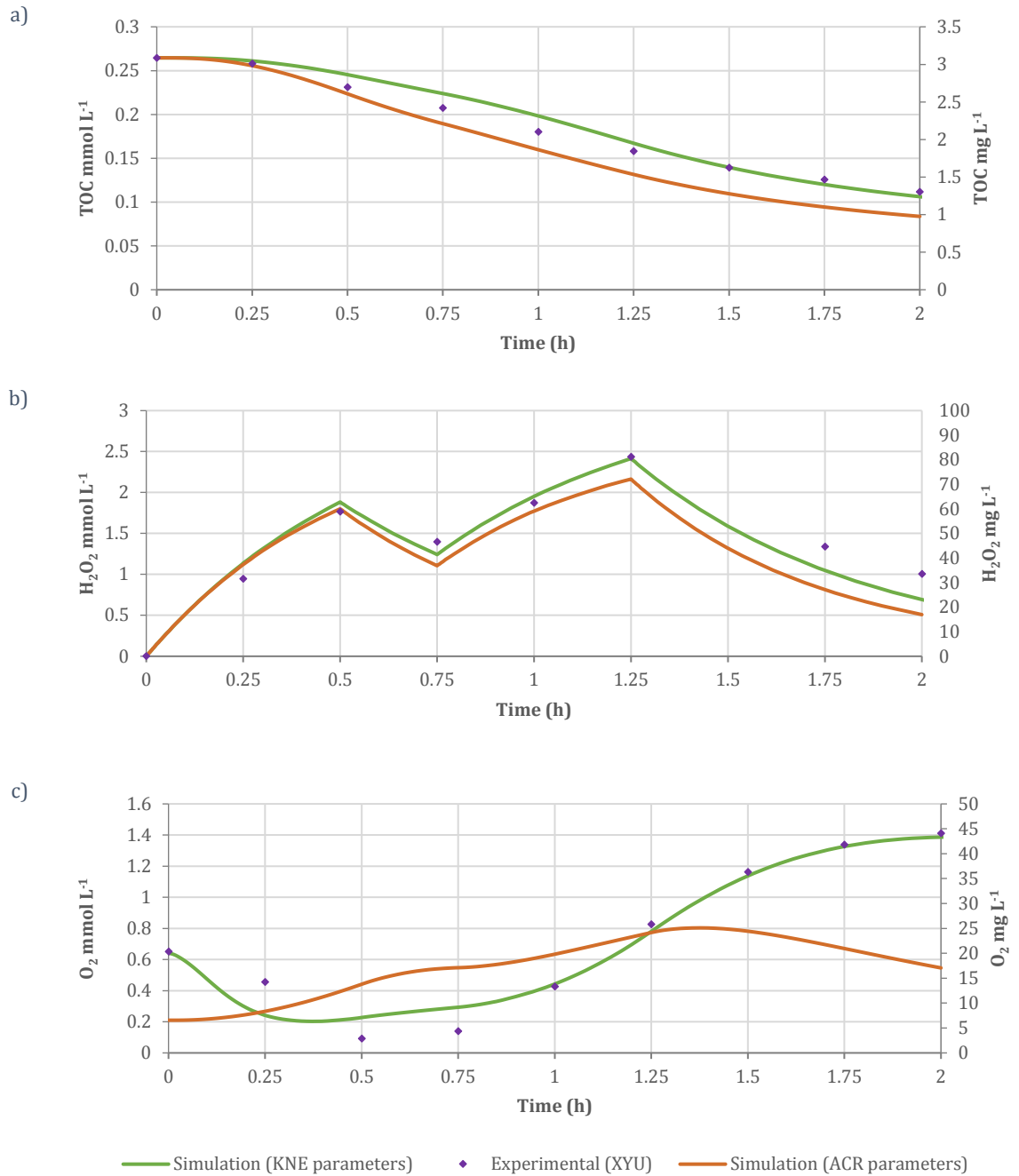


Figure 12: Experimental data (XYU) and predicted profiles (ACR and KNE) in 1011 dosage.

The results in Figure 11 and Figure 12 confirm good tuning of the fitting method, efficient performance, and ability to fit the model to the data accurately.

Figure 13 shows the ability to describe the concentration evolution of all components included in the kinetic model simulation. The simulation example corresponds to code 1111 provided in Table 1, which

has the active input flow rate from 0 to 75 minutes ($0.115 \text{ mL min}^{-1} \text{ min}$) (Figure 13a). Figure 13b shows the experimental results that would be obtained from these operational conditions. Also, the simulation provides an insight into the process by revealing the concentration of intermediates and other unobservable species: the profiles of M, MX_1 and MX_2 illustrate the transition from M to MX_1 and MX_2 (Figure 13c). This causes TOC to remain unchanged for a short period of time and then asymptotically decrease over time. As shown in the simulated profile of dissolved oxygen concentration, the concentration correlates with H_2O_2 and R levels, supporting the idea that oxygen may indicate unproductive decomposition of hydrogen peroxide.

In addition, Figure 13d presents the concentrations of all species, based on normalized values for comparison. As shown in Figure 13d, hydrogen peroxide and iron have a parallel evolution and the radical species R exhibits a delayed response in comparison with hydrogen peroxide concentration. The normalized values are calculated according to unity-based normalization as shown in Equation (29):

$$\text{Normalized } C_i = \frac{C_i - C_{\min}}{C_{\max} - C_{\min}} \quad (29)$$

The correct functioning of the model was also checked on the basis of a blank. In other words, the response of the model was analyzed when no hydrogen peroxide was added. Figure 14 shows the evolution of the concentrations of the different species of the kinetic model. In Figure 14a, where it is represented that no H_2O_2 was added, no mineralization was recorded, with TOC remaining constant. On the other hand, oxygen did decrease slightly. In Figure 14b it is shown that due to the non-addition of hydrogen peroxide, Fe^{2+} catalyst was also not consumed. As the degradation reactions do not take place, the intermediate components MX_1 and MX_2 as well as Fe^{3+} do not appear. Finally, in Figure 14d, it can be seen that the organic matter remains constant without degradation and that no radicals (R) are formed. These observations suggest once again the good behavior of the model with respect to the above-mentioned kinetic equations.

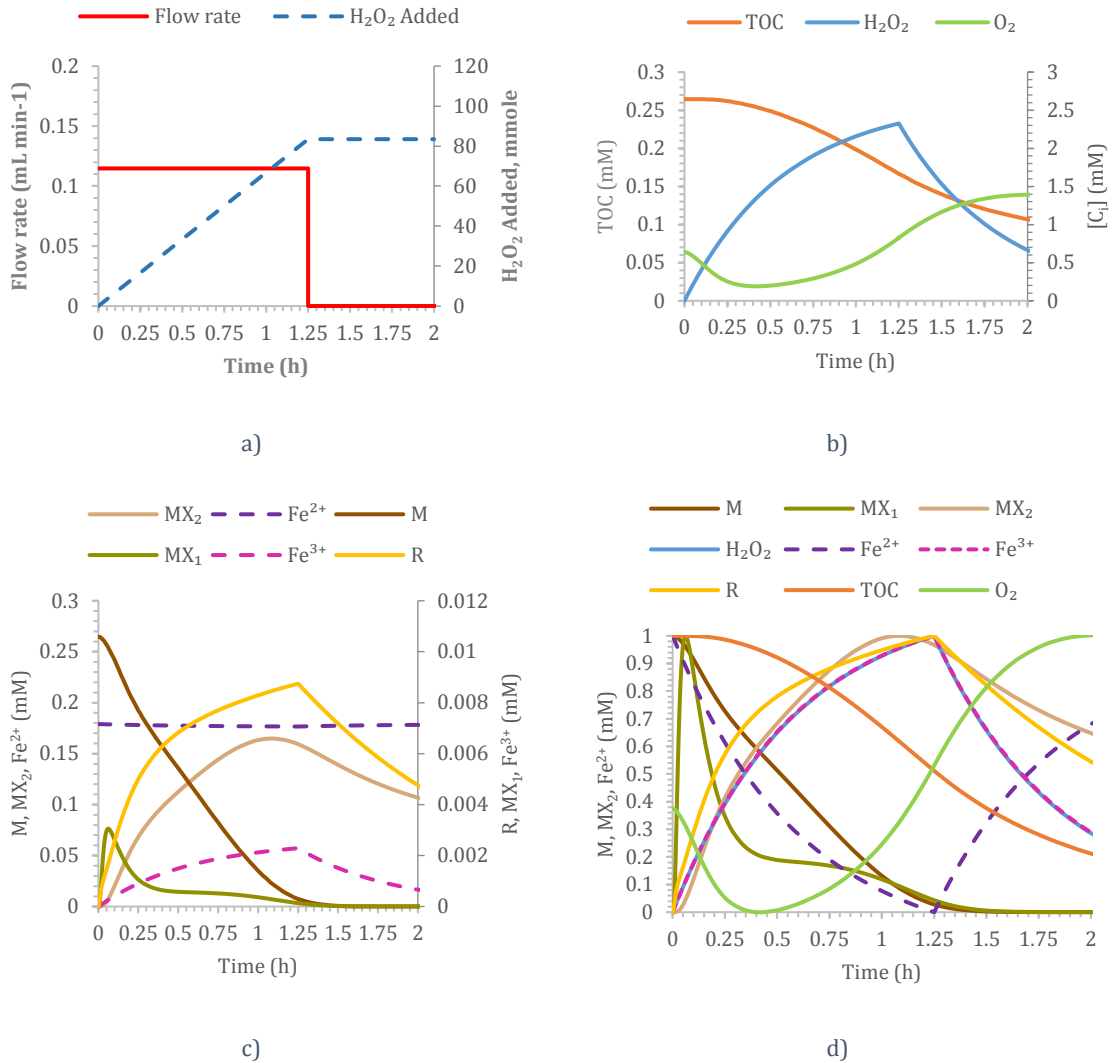


Figure 13: Simulation and concentration profiles: a) Variable H₂O₂ input profile (1111). A constant flowrate (0.115 mL min⁻¹) from 0 to 75 min. After 2h, totaling in 9.45 mL and 83.44 mmol. b) Concentration of the outputs that can be measured experimentally (O₂, TOC, H₂O₂). c) Concentration profiles for organic species (M, MX₁, MX₂), radicals (R) and iron species (Fe²⁺ and Fe³⁺). d) Concentration profile for all species (normalized).

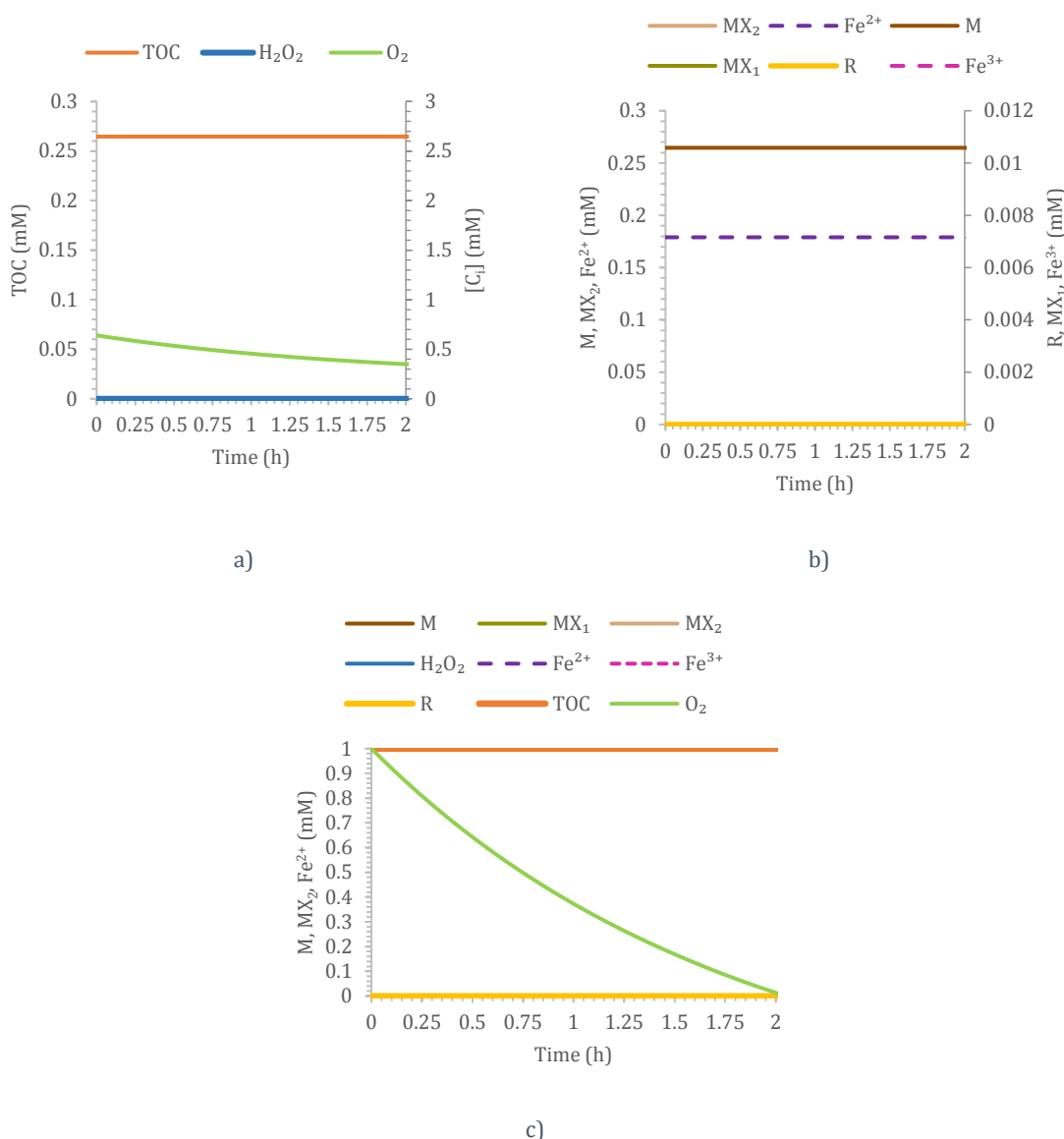


Figure 14: Simulation and concentration profile of a blank: a) Concentration of the outputs that can be measured experimentally (O_2 , TOC, H_2O_2). b) Concentration profiles for organic species (M, MX_1 , MX_2), radicals (R) and iron species (Fe^{2+} and Fe^{3+}). c) Concentration profile for all species (normalized).

This set of simulations also reveals the deeper insight that can be gained through the exploitation of the kinetic model for facilitating process understanding.

7.2 Model exploitation results and discussion

Simulation results in terms of conversion $\chi(\%)$, H_2O_2 and O_2 for different dosage profiles and different total amounts of hydrogen peroxide, A , are presented in Figure 15, Figure 16 and Figure 17, for a fixed reaction time $\tau = 6\text{h}$. In fact, the sixteen experiments performed in the pilot plant by Yu et al., (2020) reported in Table 1 were the different dosing profiles simulated. The main objective of these simulations was to see the effect on the system of increasing the total time variable, τ , and the total amount of hydrogen peroxide added, A .

In Figure 15a, the evolution of $\chi(\%)$ of the different dosages with the stoichiometric amount S , equivalent to 83.44 mmol, can be observed. Although during the first two hours there were faster dosages (i.e. No Dosage and 0000), it reached a moment, around 2.5h, where the mineralization was stabilized at a value of approximately 70% for all dosages. The same behavior was observed in Figure 15b, where the total amount of hydrogen peroxide was doubled ($2S$), equivalent to 166.88 mmol. Even so, the mineralization was stabilized around 85%. In Figure 15c, where $A=3S$ equaling 250.32 mmol, the mineralization values reached 90% after 2.5h, and neither did increase thereafter. The stabilization seems to make sense with the kinetic model used, since by not adding more H_2O_2 , the mineralization was stabilized.

The study also showed that by increasing the amount of hydrogen peroxide, the mineralization value of $\chi(\tau)$ was not reduced. Conversely, it increased when the amount of A increased. These results seem to be inconsistent with experience and the kinetic model, which show that too much hydrogen peroxide concentration could reverse the efficiency of the process by increasing the concentration of R , which will favor the reaction rate of inefficient second-order reactions.

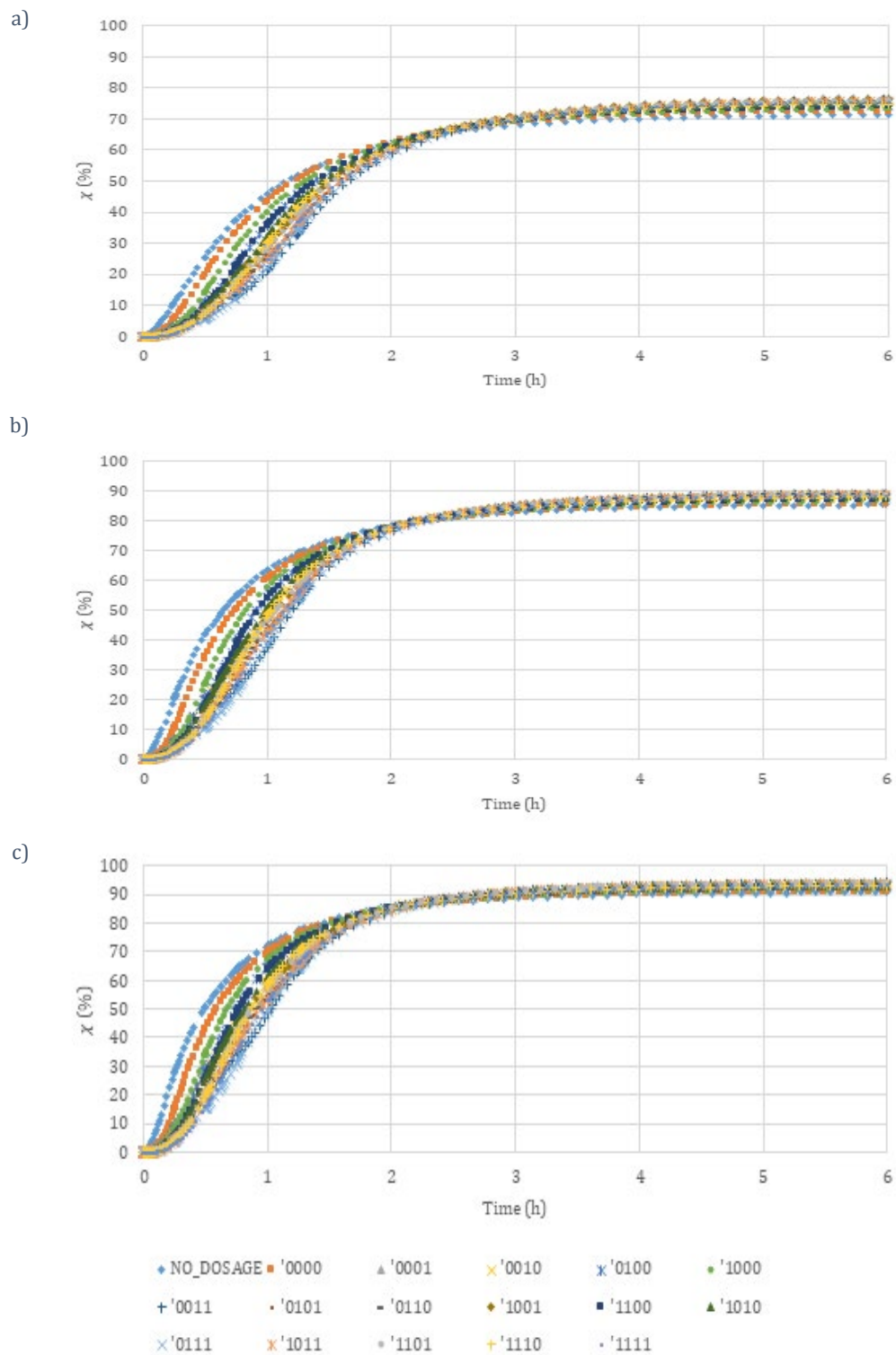


Figure 15: $\chi(\tau)$ evolution for all different dosages reported in Table 1 using different amounts of hydrogen peroxide: a) S, b) 2S, c) 3S.

The evolution of hydrogen peroxide was also analyzed from the sixteen dosing profiles (Figure 16). In Figure 16a, the stoichiometric amount S was used, in Figure 16b, $2S$ and in Figure 16c, $3S$. It can be seen how the concentration of hydrogen peroxide increased when it was added and decreased asymptotically when it was not dosed. In all three situations, it is possible to observe a pronounced decrease leading to its consumption. These graphs become interesting to check when it would be necessary to add more oxidant.

It is also important to note that once the hydrogen peroxide concentration reaches its minimum value, the TOC profile stabilizes and reaches its final value. Regarding the effect of the time increase, although it was enlarged to 6h, no significant changes were observed in the H_2O_2 evolution because no more quantity was added.

Figure 17 presents the results of the oxygen evolution of the same experiments in Table 1. Figure 17a shows the results for an amount S of hydrogen peroxide and reveals a peak in oxygen concentration for each dosage type. This increase in oxygen concentration was caused by inefficient reactions promoted by excess free radicals R due to the excess H_2O_2 concentration. A different and higher profile is observed in Figure 17 (b) and (c), where the amount of H_2O_2 was increased to $2S$ and $3S$, respectively. This result could suggest that a less efficient use of the oxidant is produced but a decrease in the final TOC removal is not observed, but the opposite.

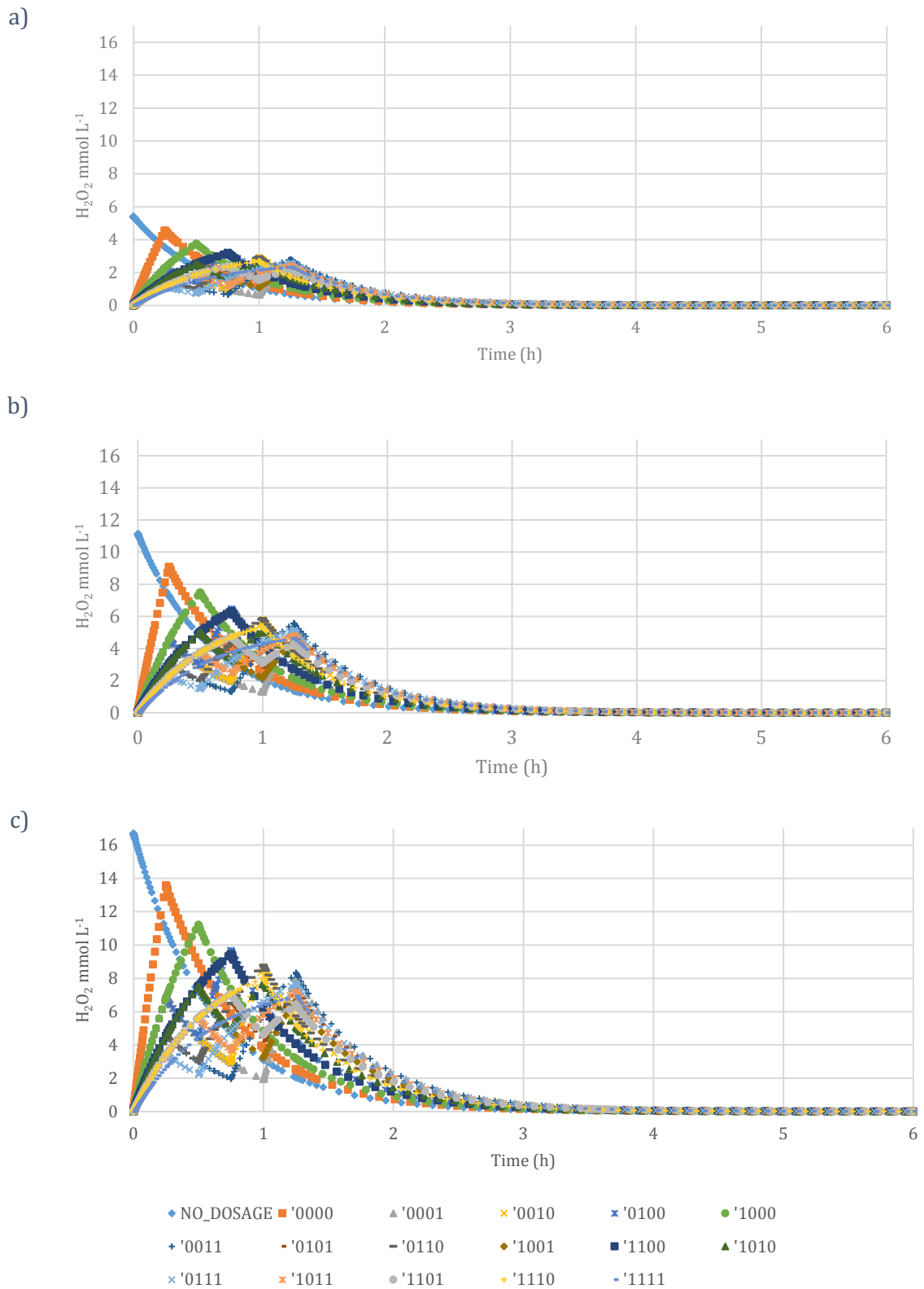


Figure 16: Hydrogen peroxide evolution for all different dosages reported in Table 1 using different amounts of hydrogen peroxide: a) S, b) 2S, c) 3S.

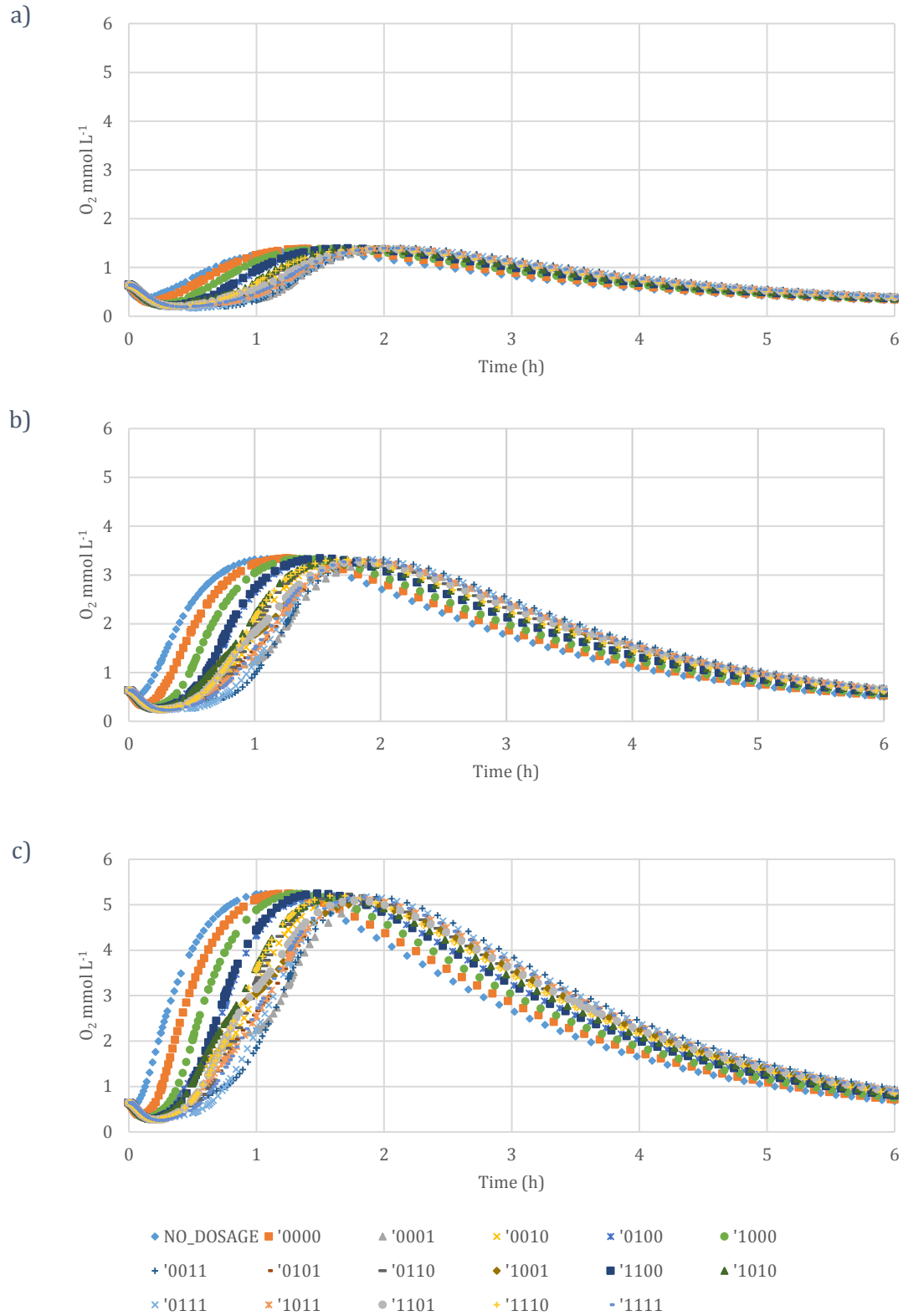


Figure 17: Oxygen evolution for all different dosages reported in Table 1 using different amounts of hydrogen peroxide: a) S, b) 2S, c) 3S.

Consequently, the H_2O_2 dosage profile is shown to not affect much the process performance since it generates similar oxygen profiles in terms of peak and similar final TOC removal.

Experience and the kinetic model used reveal the extent of inefficient reactions. These are caused by the excess concentration of hydrogen peroxide. For this reason, in order to dose hydrogen peroxide only when necessary, different simulations were performed where different constant flow rates were set and added in the first 15 minutes of reaction. After that, the dosing was kept off until the simulation showed that there was no more H_2O_2 in the system. Then, again, the same constant flow rate was dosed for another 15 minutes, waited for it to finish, and the process was repeated until approximately 100% mineralization was reached. These results are compared in terms of the time it took to reach a certain mineralization with respect to the total amount of hydrogen peroxide added (A) (Figure 18).

Figure 18 shows how a higher H_2O_2 flow rate leads to higher mineralization. Even so, with a total amount of hydrogen peroxide of 2.5S, it took more than 10h to reach 90% mineralization. This result, although H_2O_2 was supposedly used more efficiently, was no better than the results shown previously in Figure 15, where with 2S H_2O_2 amount, 90% mineralization was reached in 5h. This suggests that dosing when the H_2O_2 is finished cannot be selected as a more effective option.

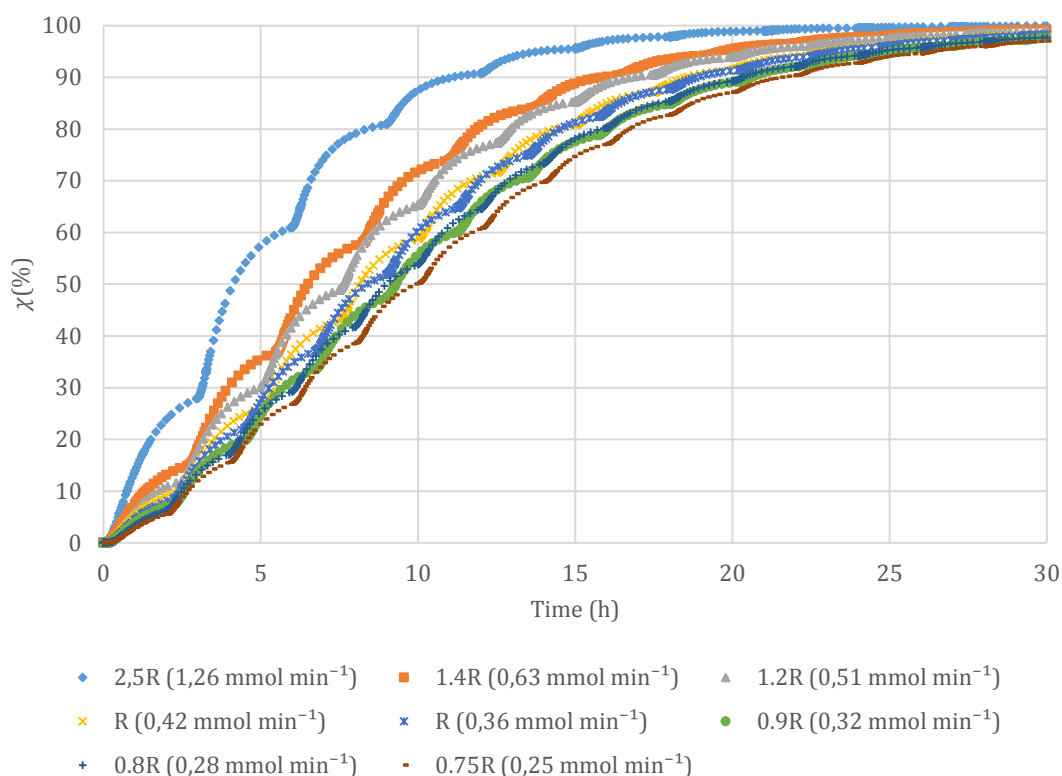


Figure 18: Study of TOC removal by adding hydrogen peroxide when it is finished in the system using different total amounts of hydrogen peroxide.

As highlighted in the state of the art, several studies on the improvement of the mineralization process in the photo-Fenton reaction have revealed the existence of an optimal dosing profile to meet the oxidation objective with the most efficient use of the oxidant. Although the model used in this project allows simulating different types of dosage, all possible dosages cannot be attempted.

Figure 19 shows a series of 50 random dosages with their corresponding $\chi(\tau)$ after a process time $\tau = 6$ h. As Yu et al., (2020) did in her experiments, the total time was divided into time spots of 15 minutes (s1 to s24). In addition, the dosing could be active (colored box) or inactive (uncolored box) i.e. the colored box indicates that H_2O_2 was constantly dosed in that time spot and, conversely, if the flow rate was deactivated, it is indicated as uncolored. The time spot s1 was always activated and dosing was established in the first 5h. The last hour was set without dosing. In all of them, the total amount of hydrogen peroxide used was S (9.45 mL, 83.44 mmol).

The final TOC removal values ranged from 70% to almost 85%. If the results were ordered from lowest to highest with respect to the $\chi(\tau)$ achieved, as shown in Figure 19, a clear pattern in the type of dosage could be seen. If H_2O_2 was added mostly at the beginning of the process, lower mineralization values were obtained, highlighting the influence of the reactant dosage on the process performance. Conversely, higher mineralization results were obtained when the dosage was more spread out over time, suggesting that a more efficient use of hydrogen peroxide was achieved.

ID	1h				2h				3h				4h				5h				6h				$\chi(\tau)$ (%)
	s1	s2	s3	s4	s5	s6	s7	s8	s9	s10	s11	s12	s13	s14	s15	s16	s17	s18	s19	s20	s21	s22	s23	s24	
1																									70,09
2																									72,47
3																									72,47
4																									72,58
5																									73,10
6																									73,95
7																									74,32
8																									75,67
9																									75,68
10																									75,68
11																									76,54
12																									76,94
13																									77,43
14																									77,82
15																									78,07
16																									78,27
17																									78,50
18																									78,78
19																									79,06
20																									79,79
21																									79,80
22																									80,38
23																									80,42
24																									80,49
25																									80,81
26																									80,98
27																									81,01
28																									81,07
29																									81,31
30																									81,70
31																									82,34
32																									82,57
33																									82,65
34																									82,74
35																									83,05
36																									83,13
37																									83,55
38																									83,65
39																									83,67
40																									83,72
41																									83,72
42																									83,82
43																									83,87
44																									83,96
45																									84,00
46																									84,10
47																									84,12
48																									84,25
49																									84,41
50																									84,73

Figure 19: Final TOC removal for 50 different random dosages.

Specifically, constant dosing is one of the best performing dosages ($\chi(\tau) = 83.65\%$), although not the best. This suggests that there is a better optimal dosage than the constant dosage that would give a higher mineralization. However, as it is mathematically complicated to find and beyond the scope of this project, constant dosing is a practical strategy that it may provide improvements in the final contaminant mineralization.

As indicated in the literature review section, hydrogen peroxide dosage strategy plays a major role in improving batch-wise operations of photo-Fenton processes. Due to inefficiency of the reactions that scavenge hydrogen peroxide, the latter is the most expensive process reactant. Consequently, the proposal of a flexible set of operating conditions (i.e. the recipe) with gradual dosage would allow the reduction or avoidance of oxidant consumption.

Consequently, different situations varying τ and A were simulated in order to obtain this recipe, with which, according to the needs of each process, suitable conditions could be chosen. Figure 20 shows the final TOC removal results of several simulations performed with dosing at constant flow rate. It was also aimed to check how much process time (τ) was needed to reach 100% mineralization given a fixed total amount of hydrogen peroxide.

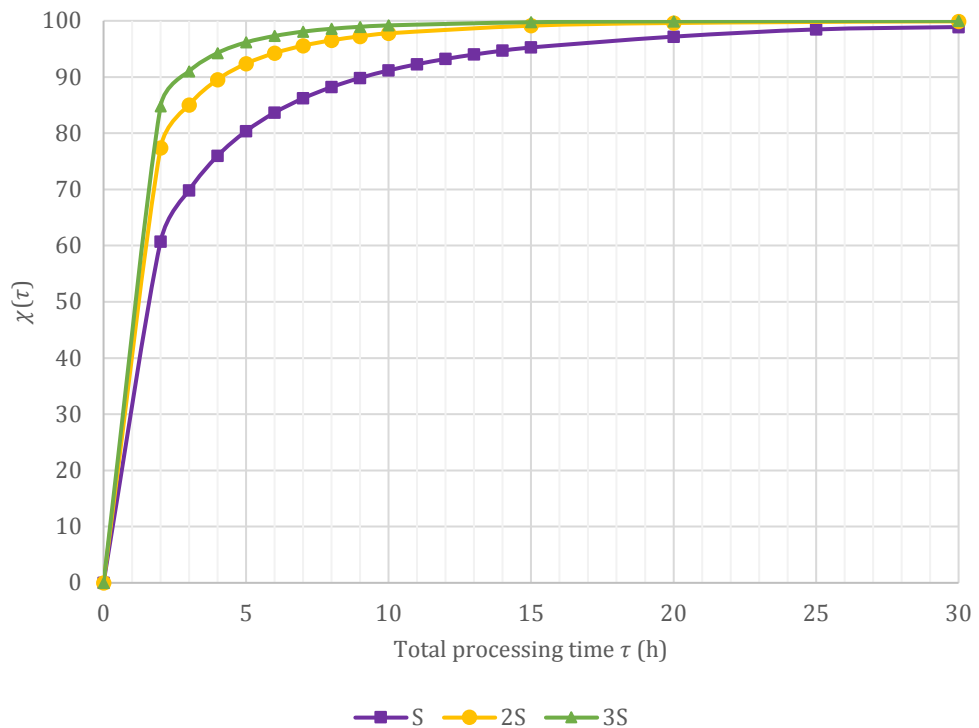


Figure 20: Final TOC removal, $\chi(\tau)$, using constant H_2O_2 flow rate and different process times (τ) and different total amounts of hydrogen peroxide ($A=S, 2S, 3S$).

In Figure 20 the results of $\chi(\tau)$ showed a strong dependence on the process time up to 5h. After that, the mineralization value tended to stabilize and gradually approach 100%. Because achieving 100% would take a very long time, mineralizations higher than 90% were considered sufficient and therefore satisfactory for this study. In all cases, using constant dosage, 90% was reached before 9h. This suggests an improvement in dosing with respect to Figure 18, where it took 20h to reach 90% with the amount S dosing H_2O_2 when it was finished in the system.

In the case of using twice the stoichiometric quantity 2S, a time of $\tau = 4$ h was necessary to obtain mineralizations of the order of 90%. In the case of 3S, just almost 3h were needed. This suggests, once again, that the addition of hydrogen peroxide leads directly to better mineralization results.

Thus, two hypotheses could be derived from Figure 20:

- on the one hand, given an amount of hydrogen peroxide, A, there was an improvement in the results of $\chi(\tau)$ when the process time τ was increased;
- on the other hand, given a process time τ , degradation ($\chi(\tau)$) increased when the total amount A was also increased.

Consequently, taking into account the studies performed and the two hypotheses proposed, two experiments were carried out on the pilot plant to verify them and try to get the recipe to obtain the operating conditions for specific needs (Table 5). It is worth it to mention that these two experiments correspond to two points selected from Figure 20:

- *Experiment 1 (EXP1)*: the total amount of hydrogen peroxide added was three times the reference amount S. Therefore, being 28.35 mL of solution, which corresponds to 567 mg L⁻¹. In this case, 2 hours was the process time (τ), using the first to dose constantly all 28.35 mL of H₂O₂ solution and the last one applying no dosage.
- *Experiment 2 (EXP2)*: the total amount of hydrogen peroxide to be dosed, A, was set to be the stoichiometric concentration (considering H₂O₂ as the only oxidant in the media), S, for the given amount of PCT: this is 9.545 g (9.45 mL of solution 30%w/v), which corresponds to a concentration of 189 mg L⁻¹ (S). The process time (τ) was 5 hours, where the first 4 hours were used to dose the 9.45 mL of solution constantly and the last hour without dosing.

7.3 Experimental results and discussion

Figure 21 and Figure 22 compare the experimental and simulated profiles as example of model performance of EXP1 and EXP2, respectively.

Figure 21 displays the evolution of the $\chi(\%)$, hydrogen peroxide and oxygen for EXP1. As expected, it shows that the model did not give a good prediction of the $\chi(\%)$ profile at the conditions tested, the difference between them being more than 20% of TOC removal at τ . Therefore, although the simulation predicted this, it has been shown that increasing the amount of H₂O₂ does not lead to better mineralization results. In this regard, the model should be adjusted. Despite that, the model was able to predict the maximum hydrogen peroxide peak, even though with some minutes of delay. With respect to the O₂ evolution, although the shape of the experimental graph was similar to that of the

simulation, the simulation estimated much higher final values. This suggests that in reality the inefficient reactions do not happen as strongly if the total amount of hydrogen peroxide is multiplied by 3. This would have to be adjusted in the model, since this estimate would be an interesting feature of the photo-Fenton process, as it is the reaction time at which the maximum availability of radical species is found.

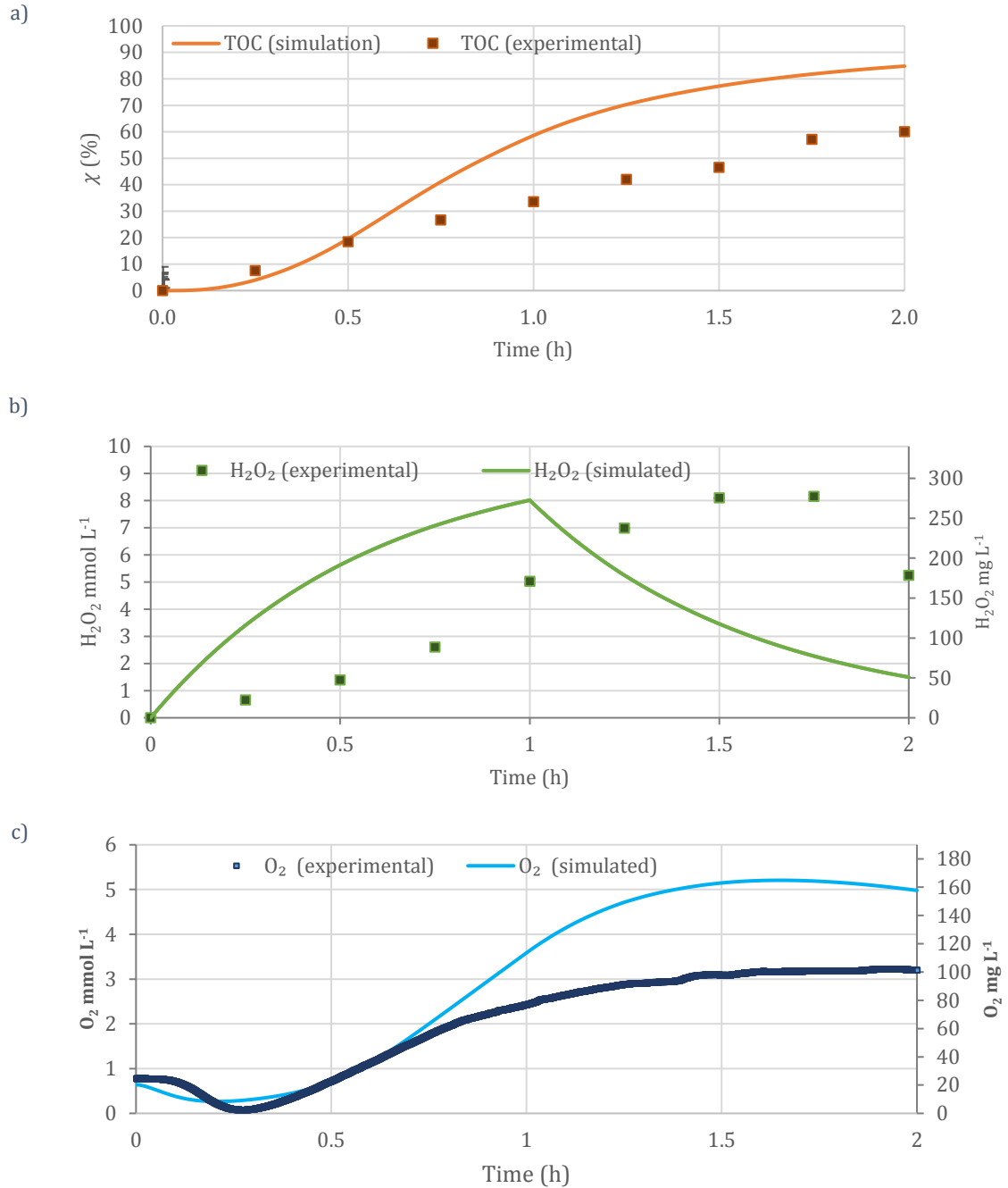


Figure 21: Experimental and simulated profiles of Experiment 1, where $\tau=2h$, $[TOC]_0=0.2646$ mmol and $A=250.3$ mmol H₂O₂.

On the other hand Figure 22 shows the evolution of $\chi(\%)$, hydrogen peroxide and oxygen in EXP2, where the total amount of H_2O_2 was the stoichiometric amount constantly dosed during 4h with $\tau = 5\text{h}$.

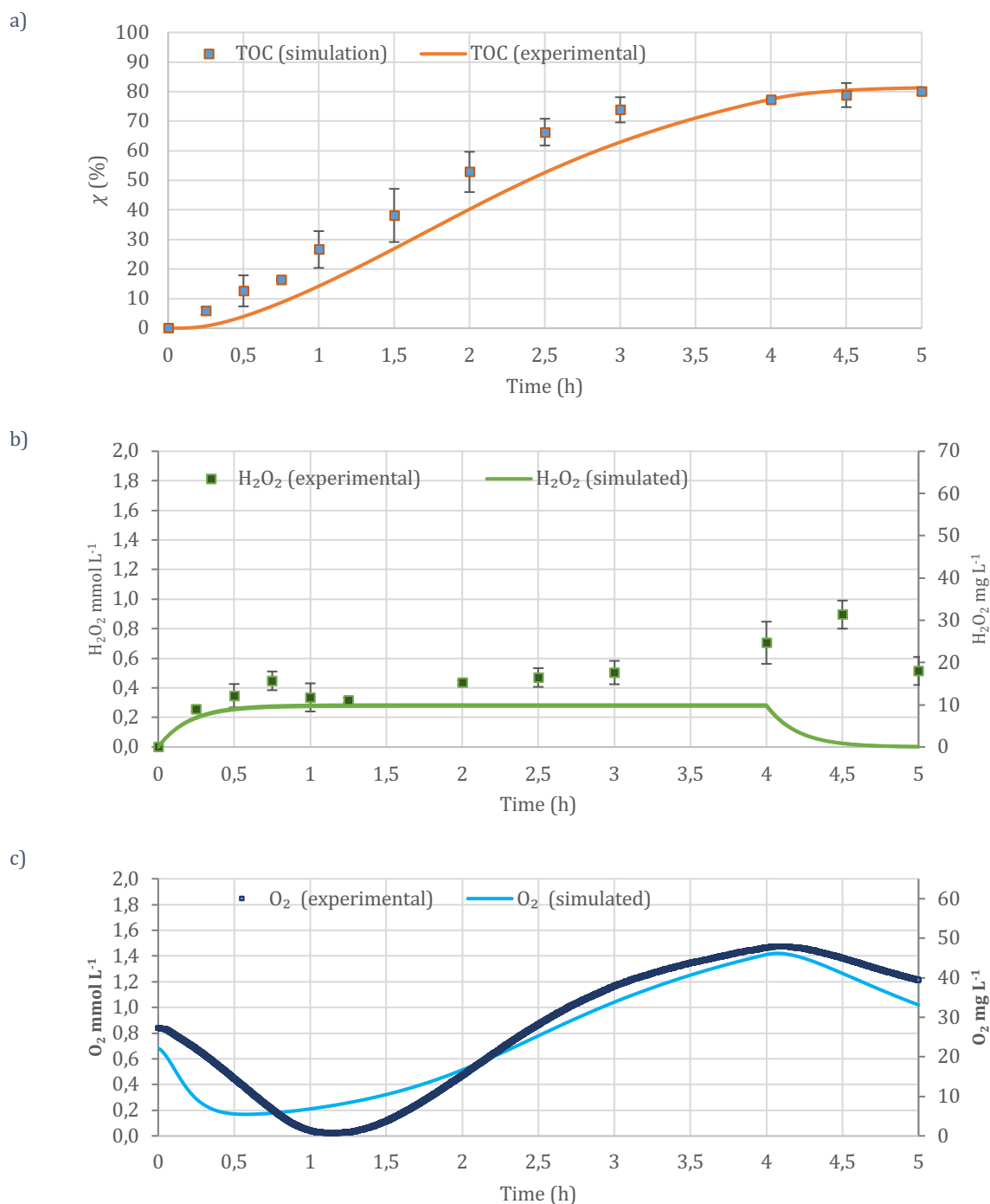


Figure 22: Experimental and simulated profiles of Experiment 2, where $\tau=5\text{h}$, $[\text{TOC}]_0=0.2646\text{ mmol}$ and $A=83.44\text{ mmol H}_2\text{O}_2$.

In the tested situation, the model was able to predict the TOC evolution very accurately, especially the final TOC (Figure 22a), being 81.3% for the simulation and 80.0% for the experimental. It was also possible to predict the evolution of hydrogen peroxide, although some adjustments should be made to the model to better predict the peak and its delay (Figure 22b).

On the other hand, with respect to the evolution of oxygen, a different situation from the one mentioned above was observed: the shape of the graph was similar and the simulation predicted very similar oxygen peak values, indicating that when the stoichiometric amount of H_2O_2 is added, the model is able to predict its evolution (Figure 22c).

The results of EXP2 revealed an improved result compared to the literature. In Yu et al., (2020), experiments, a maximum of 61.9% degradation with the stoichiometric amount of hydrogen peroxide was obtained. In this work, by constantly dosing for 4h the stoichiometric amount and with a total time of 5h, a mineralization of 80% was achieved. This was an increase of almost 20% of degradation which is worth to consider.

For simulation purposes, the model is able to show the treatment behavior of a photo-Fenton plant with given conditions while varying the operational conditions (such as the process time or the dosage profile). The mineralization and oxygen evolution can be correctly predicted for a given process when using the stoichiometric amount of H_2O_2 , as well as the hydrogen peroxide peak even though with some delay. However, analyzing situations different from those in which the model was calibrated in terms of the total amount of H_2O_2 , leads to less accurate results.

This model should be improved by adding more experiments to calibrate its parameters. Possibly, experiments with different total amounts of hydrogen peroxide would lead to a more accurate model prediction.

8 Conclusions

This study has led to an improved dosing strategy for the efficient removal of recalcitrant organic compounds with high TOC concentrations by photo-Fenton process. While experimental exploration can provide information on the efficiency of hydrogen peroxide use, it is difficult to try to improve the dosing profile because not all dosages can be tested experimentally. Consequently, this work has reached such an enhancement by systematically exploiting existing models to identify opportunities for improvement and more efficient ways of operating.

This work has exploited the dynamic photo-Fenton model by Nasr Esfahani et al., (2022), which includes flexible hydrogen peroxide dosing and has been discussed in regard of its development, fitting and validation. Hence, thanks to the reduced cost of simulations, this study has enabled the finding of dosing strategies that yield mineralization results higher than those reported in previous literature. Two improved strategies derived from simulation were then validated at a pilot plant scale.

First, an experiment used to calibrate the model was simulated using Cabrera-Reina et al., (2012) parameters as well as those fitted by Esfahani et al., (2022). As expected, the parameters fitted by Esfahani et al., (2022) were shown to more accurately describe the evolution of the process variables provided by Yu et al., (2020). In addition, they were also found to be the most accurate at estimating the final TOC removal. At this point, this fidelity of the model in describing such experimental measurements was considered satisfactory enough for undertaking model exploitation.

This was addressed by:

- Simulations of (Yu et al., 2020) experiments with longer processing time and with more hydrogen peroxide
- Simulations with more efficient dosages
- Simulations with random dosage profiles
- Simulations aimed at obtaining 100% mineralization

Yu et al., (2020) experiments were further evaluated by simulating and increase on the process time from two to six hours and an increase of the total amount of hydrogen peroxide by two and three times. Despite the longer process time, there was no significant increase in TOC removal since no more hydrogen peroxide was added. The results were more significant when the total amount of hydrogen peroxide added was increased over the reference (S). Despite inefficient reactions when more hydrogen peroxide is added, TOC removal rate increased substantially.

Due to the fact that hydrogen peroxide is more likely to produce inefficient reactions when used in excess, an attempt was made to manually dose it when most of it had been consumed. Despite the

high mineralization values, very long times were required for 90% mineralization: 15h with the total amount of hydrogen peroxide S or 10h with $2.5S$. Therefore, this option was rejected as an improvement.

A total of 50 randomly generated dosing profiles were simulated for this study with a process time of 6 hours and the stoichiometric hydrogen peroxide amount S . It evidenced that TOC removal results were improved when dosing was spread out over a longer period of time.

Hence, a subsequent strategy was proposed to determine an enhanced dosage profile. A series of constant dosage simulation runs allowed illustrating the different variables affecting process efficiency and system behavior. It was possible to show the role of hydrogen peroxide and of processing time in final TOC removal. It was observed that both an increase in process time and in hydrogen peroxide contributed to higher mineralization. By means of two different experiments, these two candidate improvements were validated in the pilot plant.

Experiment one (EXP1) showed that the prediction of the model was not very accurate when the total amount of H_2O_2 was increased by $3S$. The experiment produced a much lower mineralization rate (60.0%) than the estimated by the simulation (84.8%). This confirms Yu et al., (2020) findings that in only 2 hours, the maximum mineralization achieved is around 60%. Nonetheless, the second experiment (EXP2), which kept the total amount of hydrogen peroxide at S but increased the process time to 5h, demonstrated similarities to the model. The pilot plant assay achieved 80,0% TOC removal, while the simulation predicted 81.3%.

In both cases, the hydrogen peroxide peak was correctly predicted, although delayed. While the simulated oxygen evolution resembled the measured values in both experiments, the simulated final values were significantly higher when adding $3S$ amount (EXP1), suggesting that the model can't estimate it accurately. Despite that, the oxygen prediction was accurate for EXP2. There is a need for refinements in the H_2O_2 delay and the O_2 prediction when a different amount of S is added to the system.

This work has achieved 80% TOC removal with only the stoichiometric amount of hydrogen peroxide and with only 5h of process time when using the constant dosage studied thanks to the exploitation of the model in this study. This is approximately 20 percent points higher than the values reported by Yu et al. (2020). Moreover, the constant dosing scheme proposed to attain this performance would be an easy-to-implement solution at the production level. An extended analysis is required to further exploit and modify this model, since only some of the many dosage schemes for a photo-Fenton process have been investigated. This work has already produced promising results and practical improvements, but it is a first step towards exploiting the model for further research to find the optimal dosage strategy.

9 References

- Ahmad, A., Budi, S., Rozaimah, S., Abdullah, S., Razi, A. & Abu, H. (2022). *Chemosphere Contaminants of emerging concern (CECs) in aquaculture effluent : Insight into breeding and rearing activities, alarming impacts, regulations, performance of wastewater treatment unit and future approaches*. 290(October 2021).
- Andreozzi, R., Caprio, V., Insola, A. & Marotta, R. (1999). *Advanced oxidation processes (AOP) for water purification and recovery*. 53, 51–59.
- Antunes, S. C., Freitas, R., Figueira, E., Gonçalves, F. & Nunes, B. (2013). Biochemical effects of acetaminophen in aquatic species: Edible clams *Venerupis decussata* and *Venerupis philippinarum*. *Environmental Science and Pollution Research*, 20(9), 6658–6666. <https://doi.org/10.1007/s11356-013-1784-9>
- Audino, F. (2019). *Advanced Oxidation Process Models for Optimisation and Decision Making Support in Water Management*. June.
- Audino, F., Companyà, G., Espuña, A. & Graells, M. (2019). *Science of the Total Environment Systematic optimization approach for the efficient management of the photo-Fenton treatment process*. 646, 902–913. <https://doi.org/10.1016/j.scitotenv.2018.07.057>
- Babatunde Dauda, A., Ajadi, A., Tola-fabunmi, A. S. & Olusegun Akinwole, A. (2019). Waste production in aquaculture: Sources, components and managements in different culture systems. *Aquaculture and Fisheries*, 4(3), 81–88. <https://doi.org/10.1016/j.aaf.2018.10.002>
- Babuponnusami, A. & Muthukumar, K. (2012). Advanced oxidation of phenol: A comparison between Fenton, electro-Fenton, sono-electro-Fenton and photo-electro-Fenton processes. *Chemical Engineering Journal*, 183, 1–9. <https://doi.org/10.1016/j.cej.2011.12.010>
- Bauer, R. & Fallmann, H. (1997). *THE PHOTO-FENTON OXIDATION - A CHEAP AND TREATMENT METHOD EFFICIENT WASTEWATER*. 23(4), 341–354.
- Cabrera-Reina, A., Jordá, L. S., Sánchez, J. L. G., López, J. L. C. & Pérez, J. A. S. (2012). Applied Catalysis B: Environmental Modelling photo-Fenton process for organic matter mineralization, hydrogen peroxide consumption and dissolved oxygen evolution. *Applied Catalysis B, Environmental*, 119–120, 132–138. <https://doi.org/10.1016/j.apcatb.2012.02.021>
- da Rocha, O. R. S., Dantas, R. F., Duarte, M. M. M. B., Duarte, M. M. L. & da Silva, V. L. (2010). Oil sludge treatment by photocatalysis applying black and white light. *Chemical Engineering Journal*, 157(1), 80–85. <https://doi.org/10.1016/j.cej.2009.10.050>
- De la Cruz, N., Dantas, R. F., Giménez, J. & Esplugas, S. (2013). Photolysis and TiO₂ photocatalysis of the pharmaceutical propranolol: Solar and artificial light. *Applied Catalysis B: Environmental*, 130–131, 249–256. <https://doi.org/10.1016/j.apcatb.2012.10.003>
- Elmolla, E. S. & Chaudhuri, M. (2011). Combined photo-Fenton – SBR process for antibiotic wastewater

- treatment. *Journal of Hazardous Materials*, 192(3), 1418–1426. <https://doi.org/10.1016/j.jhazmat.2011.06.057>
- Esteves, B. M., Rodrigues, C. S. D. & Madeira, L. M. (2018). Synthetic olive mill wastewater treatment by Fenton's process in batch and continuous reactors operation. *Environmental Science and Pollution Research*, 25(35), 34826–34838. <https://doi.org/10.1007/s11356-017-0532-y>
- FAO. (2018). *MAXIMUM RESIDUE LIMITS (MRLs) AND RISK MANAGEMENT RECOMMENDATIONS (RMRs) FOR RESIDUES OF VETERINARY DRUGS IN FOODS CX/MRL 2-2018*.
- Farhataziz, A; Ross, A. B. (1977). *Selected Specific Rates of Reactions of Transients from Water in Aqueous Solution . and Their Radical Ions*.
- Göb, S., Oliveros, E., Bossmann, S. H., Braun, A. M., Nascimento, C. A. O. & Guardani, R. (2001). Optimal experimental design and artificial neural networks applied to the photochemically enhanced Fenton reaction. *Water Science and Technology*, 44(5), 339–345. <https://doi.org/10.2166/wst.2001.0321>
- Huston, P. L. & Pignatello, J. J. (1999). Degradation of selected pesticide active ingredients and commercial formulations in water by the photo-assisted Fenton reaction. *Water Research*, 33(5), 1238–1246. [https://doi.org/10.1016/S0043-1354\(98\)00330-3](https://doi.org/10.1016/S0043-1354(98)00330-3)
- Ji, F., Li, C., Zhang, J. & Deng, L. (2011). Heterogeneous photo-Fenton decolorization of methylene blue over LiFe(WO₄)₂ catalyst. *Journal of Hazardous Materials*, 186(2–3), 1979–1984. <https://doi.org/10.1016/j.jhazmat.2010.12.089>
- Jordá, L. S. J., Martín, M. M. B., Gómez, E. O., Reina, A. C., Sánchez, I. M. R., López, J. L. C. & Pérez, J. A. S. (2011). Economic evaluation of the photo-Fenton process. Mineralization level and reaction time: The keys for increasing plant efficiency. *Journal of Hazardous Materials*, 186(2–3), 1924–1929. <https://doi.org/10.1016/j.jhazmat.2010.12.100>
- Jung, Y. J., Kim, W. G., Yoon, Y., Kang, J. W., Hong, Y. M. & Kim, H. W. (2012). Removal of amoxicillin by UV and UV/H₂O₂ processes. *Science of the Total Environment*, 420, 160–167. <https://doi.org/10.1016/j.scitotenv.2011.12.011>
- Kušić, H., Koprivanac, N., Božić, A. L. & Selanec, I. (2006). Photo-assisted Fenton type processes for the degradation of phenol: A kinetic study. *Journal of Hazardous Materials*, 136(3), 632–644. <https://doi.org/10.1016/j.jhazmat.2005.12.046>
- Langford, K. H. & Thomas, K. V. (2009). Determination of pharmaceutical compounds in hospital effluents and their contribution to wastewater treatment works. *Environment International*, 35(5), 766–770. <https://doi.org/10.1016/j.envint.2009.02.007>
- Miralles-Cuevas, S., Audino, F., Oller, I., Sánchez-Moreno, R., Sánchez Pérez, J. A. & Malato, S. (2014). Pharmaceuticals removal from natural water by nanofiltration combined with advanced tertiary treatments (solar photo-Fenton, photo-Fenton-like Fe(III)-EDDS complex and ozonation). *Separation and Purification Technology*, 122, 515–522. <https://doi.org/10.1016/j.seppur.2013.12.006>
- Muir, N., Nichols, J. D., Stillings, M. R. & Sykes, J. (1997). Comparative bioavailability of aspirin and

- paracetamol following single dose administration of soluble and plain tablets. *Current Medical Research and Opinion*, 13(9), 491–500. <https://doi.org/10.1185/03007999709113322>
- Nasr Esfahani, K., Graells, M. & Pérez-Moya, M. (2022). *Science of the Total Environment Modelling of the photo-Fenton process with flexible hydrogen peroxide dosage : Sensitivity analysis and experimental validation*. 839(May). <https://doi.org/10.1016/j.scitotenv.2022.155941>
- Nichela, D. A., Berkovic, A. M., Costante, M. R., Juliarena, M. P. & García Einschlag, F. S. (2013). Nitrobenzene degradation in Fenton-like systems using Cu(II) as catalyst. Comparison between Cu(II)- and Fe(III)-based systems. *Chemical Engineering Journal*, 228, 1148–1157. <https://doi.org/10.1016/j.cej.2013.05.002>
- Nogueira, R. F. P., Oliveira, M. C. & Paterlini, W. C. (2005). Simple and fast spectrophotometric determination of H₂O₂ in photo-Fenton reactions using metavanadate. *Talanta*, 66(1), 86–91. <https://doi.org/10.1016/j.talanta.2004.10.001>
- Oller, I., Malato, S. & Sánchez-pérez, J. A. (2011). Science of the Total Environment Combination of Advanced Oxidation Processes and biological treatments for wastewater decontamination — A review. *Science of the Total Environment*, The, 409(20), 4141–4166. <https://doi.org/10.1016/j.scitotenv.2010.08.061>
- Oller, I., Malato, S. & Sánchez-Pérez, J. A. (2011). Combination of Advanced Oxidation Processes and biological treatments for wastewater decontamination-A review. *Science of the Total Environment*, 409(20), 4141–4166. <https://doi.org/10.1016/j.scitotenv.2010.08.061>
- Ortega-Gómez, E., Esteban García, B., Ballesteros Martín, M. M., Fernández Ibáñez, P. & Sánchez Pérez, J. A. (2013). Inactivation of *Enterococcus faecalis* in simulated wastewater treatment plant effluent by solar photo-Fenton at initial neutral pH. *Catalysis Today*, 209, 195–200. <https://doi.org/10.1016/j.cattod.2013.03.001>
- Ortega-gómez, E., Úbeda, J. C. M., Hervás, J. D. Á., López, J. L. C., Jordá, L. S. & Pérez, J. A. S. (2012). Automatic dosage of hydrogen peroxide in solar photo-Fenton plants : Development of a control strategy for efficiency enhancement. *Journal of Hazardous Materials*, 237–238, 223–230. <https://doi.org/10.1016/j.jhazmat.2012.08.031>
- Ortiz de la Plata, G. B., Alfano, O. M. & Cassano, A. E. (2010). Decomposition of 2-chlorophenol employing goethite as Fenton catalyst II: Reaction kinetics of the heterogeneous Fenton and photo-Fenton mechanisms. *Applied Catalysis B: Environmental*, 95(1–2), 14–25. <https://doi.org/10.1016/j.apcatb.2009.12.006>
- Pérez-Moya, M., Graells, M., Buenestado, P. & Mansilla, H. D. (2008). A comparative study on the empirical modeling of photo-Fenton treatment process performance. *Applied Catalysis B: Environmental*, 84(1–2), 313–323. <https://doi.org/10.1016/j.apcatb.2008.04.010>
- Pham, T. T. H., Brar, S. K., Tyagi, R. D. & Surampalli, R. Y. (2010). Optimization of Fenton oxidation pre-treatment for *B. thuringiensis* - Based production of value added products from wastewater sludge. *Journal of Environmental Management*, 91(8), 1657–1664. <https://doi.org/10.1016/j.jenvman.2010.03.007>

- Philips. (2022). *Actinic BL TL-DK 36W/10 1SL/25 Lámparas*.
- Pignatello, J. J. (1992). Dark and Photoassisted Fe³⁺-Catalyzed Degradation of Chlorophenoxy Herbicides by Hydrogen Peroxide. *Environmental Science and Technology*, 26(5), 944–951. <https://doi.org/10.1021/es00029a012>
- Prieto-Rodríguez, L., Oller, I., Klammerth, N., Agüera, A., Rodríguez, E. M. & Malato, S. (2013). Application of solar AOPs and ozonation for elimination of micropollutants in municipal wastewater treatment plant effluents. *Water Research*, 47(4), 1521–1528. <https://doi.org/10.1016/j.watres.2012.11.002>
- Rahim Pouran, S., Abdul Aziz, A. R. & Wan Daud, W. M. A. (2015). Review on the main advances in photo-Fenton oxidation system for recalcitrant wastewaters. *Journal of Industrial and Engineering Chemistry*, 21, 53–69. <https://doi.org/10.1016/j.jiec.2014.05.005>
- Ribeiro, A. R., Nunes, O. C., Pereira, M. F. R. & Silva, A. M. T. (2015). An overview on the advanced oxidation processes applied for the treatment of water pollutants defined in the recently launched Directive 2013 / 39 / EU. *Environment International*, 75, 33–51. <https://doi.org/10.1016/j.envint.2014.10.027>
- Sanchez-Salas, J., Flores, D. & Bandala, E. (2018). Water recalcitrant contaminants: Sources, assessment and remediation. In *Wastewater and Water Contamination: Sources, Assessment and Remediation* (pp. 1–76).
- Santos-Juanes, L., Sánchez, J. L. G., López, J. L. C., Oller, I., Malato, S. & Pérez, J. A. S. (2011). Applied Catalysis B : Environmental Dissolved oxygen concentration : A key parameter in monitoring the photo-Fenton process. *“Applied Catalysis B, Environmental,”* 104(3–4), 316–323. <https://doi.org/10.1016/j.apcatb.2011.03.013>
- Silva, A. M. T., Zilhão, N. R., Segundo, R. A., Azenha, M., Fidalgo, F., Silva, A. F., Faria, J. L. & Teixeira, J. (2012). Photo-Fenton plus Solanum nigrum L. weed plants integrated process for the abatement of highly concentrated metalaxyl on waste waters. *Chemical Engineering Journal*, 184, 213–220. <https://doi.org/10.1016/j.cej.2012.01.038>
- Taoufik, N., Boumya, W., Achak, M., Sillanpää, M. & Barka, N. (2021). Comparative overview of advanced oxidation processes and biological approaches for the removal pharmaceuticals. *Journal of Environmental Management*, 288(November 2020). <https://doi.org/10.1016/j.jenvman.2021.112404>
- Taylor, P., Pignatello, J. J., Oliveros, E. & Mackay, A. (2006). *Critical Reviews in Environmental Science and Technology Advanced Oxidation Processes for Organic Contaminant Destruction Based on the Fenton Reaction and Related Chemistry Advanced Oxidation Processes for Organic Contaminant Destruction Based on the Fent. August 2012*, 37–41. <https://doi.org/10.1080/10643380500326564>
- Ternes, T. A. (1998). Occurrence of drugs in German sewage treatment plants and rivers. *Water Research*, 32(11), 3245–3260. [https://doi.org/10.1016/S0043-1354\(98\)00099-2](https://doi.org/10.1016/S0043-1354(98)00099-2)
- Tokumura, M., Katoh, H., Katoh, T., Znad, H. T. & Kawase, Y. (2009). Solubilization of excess sludge in activated sludge process using the solar photo-Fenton reaction. *Journal of Hazardous Materials*,

- 162(2–3), 1390–1396. <https://doi.org/10.1016/j.jhazmat.2008.06.026>
- Tokumura, Masahiro, Morito, R. & Kawase, Y. (2013). Photo-Fenton process for simultaneous colored wastewater treatment and electricity and hydrogen production. *Chemical Engineering Journal*, 221, 81–89. <https://doi.org/10.1016/j.cej.2013.01.075>
- Trovó, Alam G., Pupo Nogueira, R. F., Agüera, A., Fernandez-Alba, A. R. & Malato, S. (2012). Paracetamol degradation intermediates and toxicity during photo-Fenton treatment using different iron species. *Water Research*, 46(16), 5374–5380. <https://doi.org/10.1016/j.watres.2012.07.015>
- Trovó, Alam Gustavo, Melo, S. A. S. & Nogueira, R. F. P. (2008). Photodegradation of the pharmaceuticals amoxicillin, bezafibrate and paracetamol by the photo-Fenton process-Application to sewage treatment plant effluent. *Journal of Photochemistry and Photobiology A: Chemistry*, 198(2–3), 215–220. <https://doi.org/10.1016/j.jphotochem.2008.03.011>
- Vilar, V. J. P., Moreira, F. C., Ferreira, A. C. C., Sousa, M. A., Gonçalves, C., Alpendurada, M. F. & Boaventura, R. A. R. (2012). Biodegradability enhancement of a pesticide-containing bio-treated wastewater using a solar photo-Fenton treatment step followed by a biological oxidation process. *Water Research*, 46(15), 4599–4613. <https://doi.org/10.1016/j.watres.2012.06.038>
- Wang, N., Zheng, T., Zhang, G. & Wang, P. (2016). A review on Fenton-like processes for organic wastewater treatment. *Journal of Environmental Chemical Engineering*, 4(1), 762–787. <https://doi.org/10.1016/j.jece.2015.12.016>
- Water and Sanitation | Department of Economic and Social Affairs.* (2022). <https://sdgs.un.org/topics/water-and-sanitation>
- Yamal-Turbay, E., Ortega, E., Conte, L. O., Graells, M., Mansilla, H. D., Alfano, O. M. & Pérez-Moya, M. (2015). Photonic efficiency of the photodegradation of paracetamol in water by the photo-Fenton process. *Environmental Science and Pollution Research*, 22(2), 938–945. <https://doi.org/10.1007/s11356-014-2990-9>
- Yu, X., Cabrera-Reina, A., Graells, M., Miralles-Cuevas, S. & Pérez-Moya, M. (2021). Towards an efficient generalization of the online dosage of hydrogen peroxide in photo-fenton process to treat industrial wastewater. *International Journal of Environmental Research and Public Health*, 18(24). <https://doi.org/10.3390/ijerph182413313>
- Yu, X., Somoza-Tornos, A. & Graells, M. (2020). *Science of the Total Environment An experimental approach to the optimization of the dosage of hydrogen peroxide for Fenton and photo-Fenton processes.* 743. <https://doi.org/10.1016/j.scitotenv.2020.140402>
- Zapata, A., Oller, I., Rizzo, L., Hilgert, S., Maldonado, M. I., Sánchez-Pérez, J. A. & Malato, S. (2010). Evaluation of operating parameters involved in solar photo-Fenton treatment of wastewater: Interdependence of initial pollutant concentration, temperature and iron concentration. *Applied Catalysis B: Environmental*, 97(1–2), 292–298. <https://doi.org/10.1016/j.apcatb.2010.04.020>
- Zhang, Y. & Pagilla, K. (2010). Treatment of malathion pesticide wastewater with nanofiltration and photo-Fenton oxidation. *Desalination*, 263(1–3), 36–44.

<https://doi.org/10.1016/j.desal.2010.06.031>



